

---

# MAREO: MEMORY AND ATTENTION BASED VISUAL REASONING

---

A PREPRINT

Mohit Vaishnav<sup>1,2,3</sup> and Thomas Serre<sup>1,2</sup>

<sup>1</sup>Artificial and Natural Intelligence Toulouse Institute, Université de Toulouse, France

<sup>2</sup>Carney Institute for Brain Science, Dpt. of Cognitive Linguistic & Psychological Sciences, Brown University, Providence, RI 02912

<sup>3</sup>Centre de Recherche Cerveau et Cognition, CNRS, Université de Toulouse, France

## ABSTRACT

Humans continue to outperform modern AI systems in their ability to parse and understand complex visual scenes flexibly. Attention and memory are two systems known to play a critical role in our ability to selectively maintain and manipulate behaviorally-relevant visual information to solve some of the most challenging visual reasoning tasks. Here, we present a novel architecture for visual reasoning inspired by the cognitive-science literature on visual reasoning, the Memory- and Attention-based (visual) REasOning (*MAREO*) architecture. *MAREO* instantiates an active-vision theory, which posits that the brain solves complex visual reasoning problems compositionally by learning to combine previously-learned elementary visual operations to form more complex visual routines. *MAREO* learns to solve visual reasoning tasks via sequences of attention shifts to route and maintain task-relevant visual information into a memory bank via a multi-head transformer module. Visual routines are then deployed by a dedicated reasoning module trained to judge various relations between objects in the scenes. Experiments on tasks containing complex visual relations (SVRT (Fleuret et al., 2011)) and same-different differentiation, relation match to sample, Raven’s and Identity rules from ART (Webb et al., 2021) demonstrate *MAREO*’s ability to learn visual routines in a robust and sample-efficient manner. We also show the zero-shot generalization on unseen tasks and the compositionality nature of the architecture.

## 1 Introduction

Intelligence is not only the ability to reason but also to find relevant material in memory and deploy attention when needed.

*Daniel Kahneman*

Abstract reasoning is fundamental to general intelligence in humans and animals (Gentner and Markman, 1997; Lovett and Forbus, 2017) helping to understand the world. It is the ability to analyze information and discover rules to solve any given task. Such abstract reasoning ability in neural networks is evaluated with the help of datasets like Raven’s Progressive Matrices (RPM) (Barrett et al., 2018; Zhang et al., 2019), SVRT (Fleuret et al., 2011) constituting seven and twenty-three unique relations, respectively. However, Raven’s dataset has a critical issue allowing models to cheat the task (Hu et al., 2020; Spratley et al., 2020). Another recently proposed dataset, Abstract Reasoning Task (ART) (Webb et al., 2021), introduced four visual reasoning challenges to evaluate neural networks. An increasingly large body of literature shows that feedforward neural architectures exhibit significant limitations in their ability to solve relatively simple visual cognitive tasks. This is where progress needs to be made.

Given the vast superiority of animals over state-of-the-art AI systems, it makes sense to turn to neuroscience to find inspiration for extending modern deep neural networks with brain-like mechanisms that would improve their ability to solve visual reasoning tasks. Indeed, a recent human EEG study has shown that attention and memory processes are

needed to solve same-different visual reasoning tasks (Alamia et al., 2021). Consistent with this finding, recent work has provided further computational evidence regarding the benefits of attention in solving many of the most challenging visual tasks in the Synthetic Visual Reasoning Tasks (SVRT) challenge (Messina et al., 2021a; Vaishnav et al., 2022). Similarly, computational evidence regarding the benefits of memory has recently emerged for learning abstract relations with a limited number of training samples (Webb et al., 2021). However, these two lines of work demonstrating the benefits of attention and memory for visual reasoning were evaluated based on different visual reasoning datasets and different base architectures, making any comparison impossible. Overall, while previous work has suggested that attention and memory mechanisms are helpful for visual reasoning, the relative contributions of these two mechanisms remain poorly understood.

Here, we aim to fill this gap and describe an integrated neural architecture called *MAREO* (Memory- and Attention-based visual REasOning). One of the key features in MAREO is a cognitive controller which learns visual routines that sequentially guide attention to task-relevant locations and gate the corresponding visual elements into a memory where they are stored and actively maintained as “context vectors” and subsequently manipulated by a relational reasoning module that has learned to judge object relations. Through experiments on two visual reasoning datasets, we demonstrate that our neural architecture is capable of learning complex compositions of relational rules in a data-efficient manner and performs better than other existing feedforward architectures. Using explainability methods, we further characterize the reasoning strategies discovered by the model in order to solve representative SVRT tasks. We demonstrate that our model is compositional – in that it is able to generalize to novel tasks efficiently and learns novel visual routines by re-arranging previously learned elementary operations.

**Contributions** Our contributions are as follows:

- We describe an end-to-end trainable model endowed with a novel memory and guided-attention system to learn to solve multiple visual reasoning tasks in a data-efficient manner.
- We show that our guided-attention module, controlled by a multi-head transformer module, learns to shift attention to task-relevant locations and gate relevant visual elements into memory and performs better than the so popular self-attention mechanisms.
- We provide empirical evidence that attention is necessary for selecting relevant visual areas, while memory is needed for storing them.
- We show that our architecture demonstrates compositional behavior and learns to adapt to a novel scenario by rearranging already-learned elementary operations within its reasoning module.
- Our architecture sets a new benchmark on two visual reasoning datasets SVRT (Fleuret et al., 2011) and Abstract Reasoning Task (ART) (Webb et al., 2021).

## 2 Proposed approach

**Theoretical framework** Visual routine theory Ullman (1984, 1987) serves the basis of the framework in our proposed model. According to this theory, visual processing can be divided into three stages. In the first stage, *base representation* is created for the input in a bottom-up manner. Once this representation is created, a sequence of elemental operations is applied to the base representation in the second stage. Some of these elemental operations are listed as follows (this list is not exhaustive):

- *Shift of processing focus*: This process is similar to the spotlight of selective attention, which helps to shift the processing focus on the image from one part to the other.
- *Indexing*: It enlists all locations where processing focus can shift.
- *Assembly*: Routines are generally generated in response to some internal queries by assembly mechanism in response to specific goals.

These sequences of elemental operations are known as *visual routines* and are used to create *incremental representations* from the already available base representation. Finally, these incremental representations are used in the third stage to reason about the task. We have added more details in SI S2.

**Architecture** Inspired by the framework mentioned above, our model can be divided into three components: an encoder, a controller, and a relational module (see Fig. 1 for an overview).

The **encoder module** includes a feature extraction block ( $f_e$ ) for an image ( $x_{in}$ ) which is composed of five convolutional blocks (Fig. S6). The output of the module is denoted as  $z_{img} \in \mathcal{R}^{(128,hw)}$  (with  $h$  height and  $w$  width). This

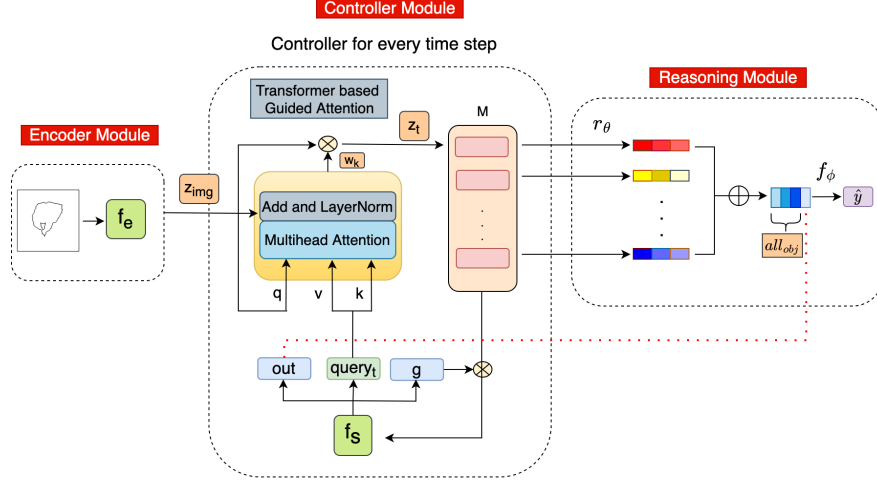


Figure 1: Our proposed *MAREO* architecture is composed of three components: an *encoder* module builds a visual representation of an image, a *controller* module controls a transformer-based multi-head attention layer to shift attention and selectively routes task-relevant object representations to be stored in a memory bank ( $M$ ). The controller uses query vectors at each time step to guide the next shift of attention based on the current fixation. After a few shifts of attention, a reasoning module learns to identify the relationships between context vectors stored in memory.

representation is equivalent to the *base representation*. To better understand the relations at the image level, we applied Temporal Context Normalization (TCN) (Webb et al., 2020). This type of normalization is applied at the task-relevant window (a single image in our case). Applying TCN helps preserve the relational information between the objects within the window, resulting in better learnability. TCN is applied over this representation before passing  $z_{img}$  for further processing.

After this base representation is built, a *guided-attention* block routes visual information from relevant image location at each time step ( $t$ ). This block builds on the now classic *multi-head attention* (MHA) transformer module used in Natural Language Processing (Vaswani et al., 2017), which differs substantially from the self-attention transformer module more commonly used in vision. An MHA block works as a retrieval block to extract relevant information based on 3 attention variables: key ( $k$ ), query ( $q$ ) and value ( $v$ ). The query ( $q$ ) is used to compute a similarity score with the key ( $k$ ), which is then multiplied by the values ( $v$ ). In our implementation, MHA accepts keys and values from a controller ( $f_s$ ), discussed in the next paragraph and queries from the encoder block ( $f_e$ ) to generate a weight vector ( $w_k \in \mathcal{R}^{128}$ ) corresponding to the key ( $k$ ). The vectors  $w_k$  is then used to modulate the feature vector  $z_{img}$  to yield a new context vector ( $z_t \in \mathcal{R}^{128}$ ). A similar approach was used in Visual Question Answering (*VQA*) (Yu et al., 2019) to compute the similarities between questions and images. The context vector ( $z_t$ ) is then stored in the memory bank ( $M$ ) for further deriving the relational vector in the reasoning module. This memory bank is inspired by the differential memory in Webb et al. (2021).

The **controller module** helps in the implementation of sequences of operation like shifting of attentional focus and generating query ( $query_t$ ) as a response to a task-specific goal. These operations generate incremental representations ( $z_t$ ). Controller module uses an Long Short-Term Memory (LSTM) as a controller ( $f_s$ ) which provides the query vector ( $query_t \in \mathcal{R}^{128}$ ) as input to the attention module for the current time step  $t$ . The controller  $f_s$  is also responsible for updating the gain vector of the feature channel ( $g \in \mathcal{R}^{128}$ ) and output vector ( $out \in \mathcal{R}^{512}$ ).  $g$  is multiplied with the context vectors stored in  $M$  at time step  $t - 1$  to generate the next input for the controller  $f_s$ . In the controller block, a query generated from recurrent module  $f_s$  is used to route the guided-attention block to the task-relevant features to be saved in memory block  $M$ . Gating ( $g$ ) is later used to shift to the next task-relevant feature based on the features previously stored in  $M$ .

A **relational module** is where the reasoning takes place over the incremental representations ( $z_t$ ) stored in the memory bank ( $M$ ). We implement this module with the help of a multilayer perceptron (MLP) layer ( $r_\theta$ ) which gives us a relational vector ( $all_{obj}$ ) similar to a Relational network (Santoro et al., 2017). As we will show (section 4.3),  $r_\theta$  learns elementary operations to make basic relational judgments between context vectors stored in the memory ( $M$ ). These elemental representations are arranged, and a task-relevant rule is learned as a relational vector ( $all_{obj}$ ). It is concatenated with the output ( $out$ ) of the controller ( $f_s$ ) at the last time step ( $t=T$ ) and passed through  $f_\phi$  to take the decision ( $\hat{y}$ ) for a particular task. We have summarized the steps in Algorithm 1 in SI.

## 3 Experiments

### 3.1 Dataset

**ART** Webb et al. (2021) proposed four types of visual reasoning tasks (Figure S23) that we will henceforth refer to as the *Abstract Reasoning Task* (ART): (1) a same-different (*SD*) discrimination task, (2) a relation match to sample task (*RMTS*), (3) a distribution of three tasks (*Dist3*) and (4) an identity rule task (*ID*). These four tasks utilize shapes from a set of 100 unique Unicode character images<sup>1</sup>. They are divided into training and test sets into four generalization regimes using different holdout character sets ( $m = 0, 50, 85, \text{ and } 95$ ) from 100 characters. We have described training and test samples and different hyperparameters for all four tasks in SI. (section S6).

**SVRT** In contrast to the ART tasks, which focus on generalization to novel shapes and sample efficient learning, SVRT tests a greater number of rules applied to more complex shapes. SVRT dataset is composed of 23 different binary classification challenges, each representing either a single rule or a composition of multiple rules. A complete list of tasks with sample images from each category is shown in SI (Figures S19, S20). We formed four different datasets with 0.5k, 1k, 5k, and 10k training samples to train our model. We used unique sets of 4k and 40k samples for validation and test purposes. Classes were balanced for all analyses.

### 3.2 Baseline models

**ART** As a baseline, we chose the ESN (Webb et al., 2021) along with the two other prevalent reasoning architectures, the Transformer (Vaswani et al., 2017) and Relation Network (RN) (Santoro et al., 2017). These three share a similar encoder backbone as in *MAREO*. In order to make our baselines stronger, we evaluated these models in their natural order, i.e., by passing a single image at a time. We added a random translation for the shapes in the area of  $\pm 5$  pixels around the center to prevent these architectures from performing template matching. In comparison, for *MAREO* we present task-relevant images together as a single stimulus (SI, Fig. S24). We have also added ART results where each image is center-shifted and put together in a single stimulus in SI section S7. In order to make our architecture choose one option from multiple stimuli (*RMTS*: 2, *Dist3* or *ID*: 4), we concatenate the relational vector ( $all_{obj}$ ) for every stimulus and pass them to a linear layer for final decision.

**SVRT** For the baselines in this dataset, we compared our architecture performance to a Relational Network (*RN*), a popular architecture for reasoning in VQA. The *RN* uses the same CNN backbone as *MAREO* with feature maps of dimension  $\mathcal{R}^{128,hw}$  where  $h = 8$  and  $w = 8$ . We consider each spatial location of the encoded feature representation as an object (i.e.,  $N = 8 \times 8 = 64$  object representations). We computed all pairwise combinations between all 64 representations using a shared MLP between all the possible pairs (4096 pairs). These combinations were then averaged and processed through another MLP to compute a relational feature vector before the final prediction layer ( $f_\phi$ ). In a sense, *MAREO* is a special case of an *RN* network endowed with the ability to attend to a task-relevant subset ( $N = 4$ ) of these representations with the help of a controller instead of exhaustively computing all 4,096 possible relations – thus reducing the computing and memory requirements of the architecture very significantly.

As an additional baseline model we used ResNet-50 (He et al., 2016) (*R50*) and its transformer-based self-attention network (*Attn-R50*) introduced in Vaishnav et al. (2022). These have been previously evaluated on SVRT tasks (Funke et al., 2021; Vaishnav et al., 2022; Messina et al., 2021b,a). It serves as a powerful baseline because of more free parameters and a self-attention module to compare the proposed active attention component of *MAREO*. In our proposed method, the controller shifts attention heads sequentially to individual task-relevant locations against a more standard self-attention module where all task-relevant locations are attended simultaneously. We also evaluated ESN in which we used a similar encoder to that of *MAREO* and passed the images in sequential order with each shape as a single stimulus and number of time steps as the number of shapes present in the SVRT task. In order to train these models we used images of dimension  $128 \times 128$  for architectures such as *RN*, *ESBN*, *MAREO* and  $256 \times 256$  for *R50*, *Attn-R50* (to be consistent with previous work).

## 4 Results

### 4.1 Task-level performance

**SVRT** All twenty-three tasks in this dataset can be broadly divided into two categories, same-different (*SD*) and spatial relations (*SR*), based on the identification of relations. Same-different (*SD*) tasks (7, 21, 5, 19, 6, 17, 20, 1, 13,

<sup>1</sup>[https://github.com/taylorwebb/emergent\\_symbols](https://github.com/taylorwebb/emergent_symbols)

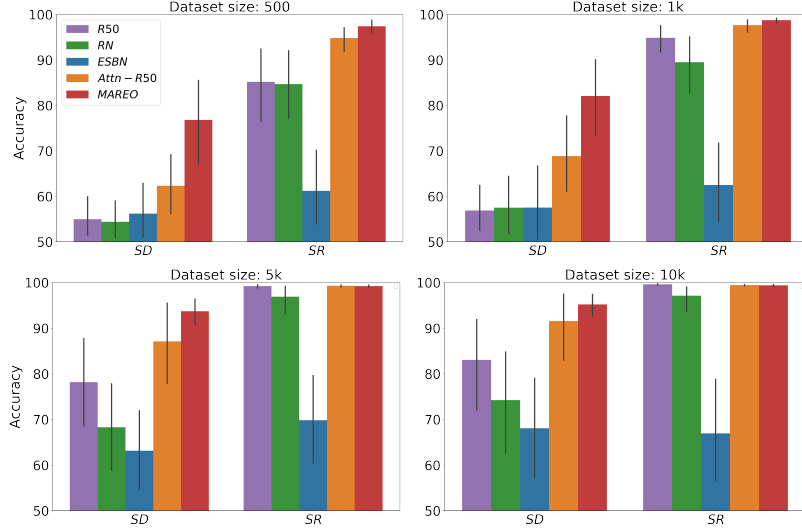


Figure 2: Bar plot analysis for the SVRT tasks grouped in same-different (*SD*) and spatially related (*SR*) tasks. We compared the accuracies of five baseline architectures with *MAREO*. ResNet-50 (*R50*) has 23M parameters, Relation Network (*RN*) has 5.1M parameters, ResNet-50 with attention (*Attn-R50*) has 24M parameters and *MAREO* & *ESBN* both have 6.6M parameters. We trained these with .5k, 1k, 5k and 10k samples.

22, 16) have been found to be harder for neural networks (Ellis et al., 2015; Kim et al., 2018; Stabinger et al., 2016, 2021; Puebla and Bowers, 2021; Messina et al., 2021a; Vaishnav et al., 2022) compared to spatial relations (*SR*) tasks (12, 15, 14, 9, 23, 8, 10, 18, 4, 3, 11, 2).

We analyzed an array of architectures and found that, on average, *MAREO* achieves at least 15% better test accuracy score on *SD* tasks for 500 samples, while for *SR* tasks, average accuracy has already reached perfection. We find a similar trend for other architectures when trained with different dataset sizes. Overall, RN (*MAREO* minus attention) and *ESBN* struggled to solve SVRT tasks even with 10k training samples, pointing towards the lack of an essential component, such as attention. On the other hand, *Attn-R50* architecture demonstrated the second-best performance, which shows its importance in visual reasoning.

**ART** For all the baseline models and in different generalization scenarios, we observed a near-chance level accuracy for the *SD* and *RMTS* tasks. In order to validate the encoder of the *ESBN* architecture, we trained it when the images were centered in the *SD* task, which resulted in perfect accuracy, probably via template matching. To further strengthen our claim, we also analyzed *ESBN* in the presence of Gaussian noise (0 mean and .05 variance) and found a similar chance level accuracy for the *SD* task (Fig. S26). It shows that attention is required for solving the same-different and related tasks. For the other two tasks *Dist3* and *ID*, baseline models performed better than the chance level (25%). *ESBN* showed an increasing trend in accuracy for progressively easier generalization conditions approaching 0 holdouts. This points toward the fact that the first three shapes in both these tasks allow *ESBN* to consider a translation factor while comparing the next three shapes, letting it choose the correct option accordingly. RN and Transformer still struggled to generalize.

## 4.2 Learning rules

We hypothesize that if a model has learned the abstract rule underlying a given task, it should be able to re-use its knowledge of this task on other novel tasks which share a similar rule. To verify that *MAREO* is indeed able to generalize across tasks that share similar rules, we searched for pairs of tasks in SVRT which were composed of at least one common elementary relation (Vaishnav et al., 2022) between them. For example, in pair (1, 22), task 1 involves the identification of two similar shapes in category 1 and task 22 involves the identification of three similar shapes in category 1. In the selected pair, the category that judges the similar rule should belong to the same class (let us say category 1 in the above example) so that we test for the right learnability. We systematically identified a set  $x$  of tasks 1, 5, 7, 21, 23 representing elementary relations such as identifying same-different (1, 5), grouping (7), learning transformation like scaling and rotation (21) and learning insiderness (23). Then we paired them with other tasks sharing similar relations. These pairs are task 1 with each of 5, 15 and 22, task 5 with each of 1, 15 and 22. Similarly other pairs

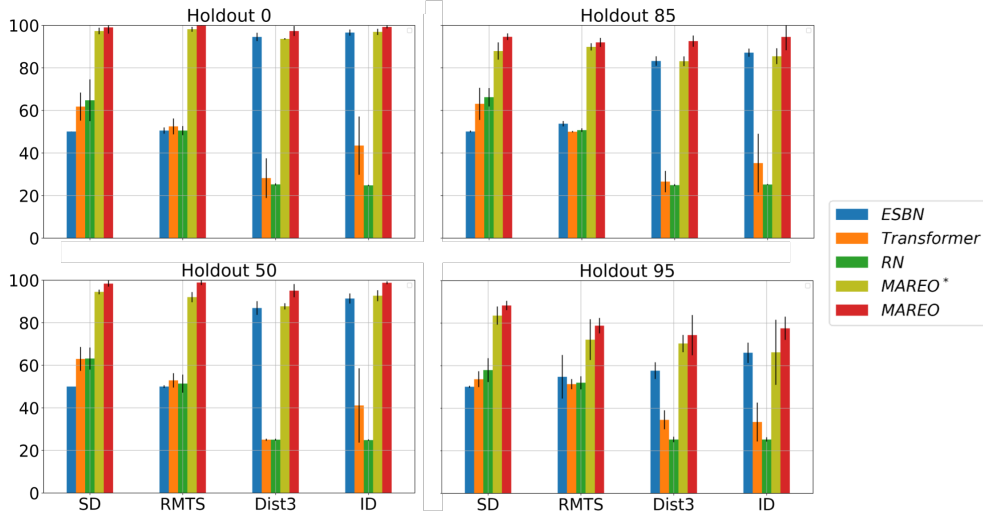


Figure 3: **ART**: Comparing the average performance of *MAREO* with ESNB, Transformer and Relational Network (RN) over 10 runs for different holdout values ( $m = 0, 50, 85, 95$ ). *MAREO\** is the setup where all the shapes in a stimulus are presented together and also shifted thereby adding more degree of complexity (refer to SI). These models are evaluated on four types of tasks, i.e., Same-Different (SD), Relation match to sample (RMTS), Distribution of 3 (Dist3) and Identity rules (ID).

Training Task	Test Task	Test Accuracy		
		MAREO	Attn-R50	R50
1	5	72.07	53.03	<b>73.04</b>
	15	<b>92.53</b>	92.07	78.87
	22	<b>84.91</b>	80.10	67.15
5	1	<b>92.64</b>	85.73	92.28
	15	<b>84.36</b>	62.69	49.95
	22	<b>76.47</b>	55.69	50.19
7	22	<b>83.80</b>	79.11	50.37
21	15	<b>90.53</b>	50.00	49.76
23	8	<b>85.84</b>	58.90	59.25

Table 1: Test accuracy to show if the model learns the correct rules when we train it with a task and test on a different set of SVRT tasks with *MAREO*, Attention with ResNet50 (Attn-R50) and ResNet-50 (R50).

of tasks are (7, 22), (21, 15) and (23, 8). We have explained how all these pairs of tasks form a group in SI section S1.2. We separately trained the model on the set  $x$  and tested the same model on their respective pairs without finetuning further with any samples from the test set (zero-shot classification).

We observed that *MAREO* is easily able to generalize from one task to another without any re-training. On the contrary, a chance level accuracy by ResNet-50 (R50) shows the network’s rote memorization of task-dependent features. In comparison, *MAREO* exhibits far greater abstraction abilities – demonstrating an ability to comprehend rules in unseen tasks without any training at all. We further explored the strategies learned by *MAREO* using attribution methods for all the tasks (see SI section S4). These attribution methods confirm that *MAREO* does indeed use a similar visual routine between the original task for which it was trained and the new task for which it was never trained. Table 1 summarizes all the results.

### 4.3 Learning Compositionality

Below, we provide evidence that *MAREO* is capable of harnessing compositionality. We looked for triplets of tasks  $(x, y, z)$  such that  $z$  would be a composition of tasks  $x$  and  $y$ . We systematically looked for all such available triplets in the SVRT dataset and found three of them (15, 1, 10), (18, 16, 10) and (21, 19, 25). All these tasks and their associated

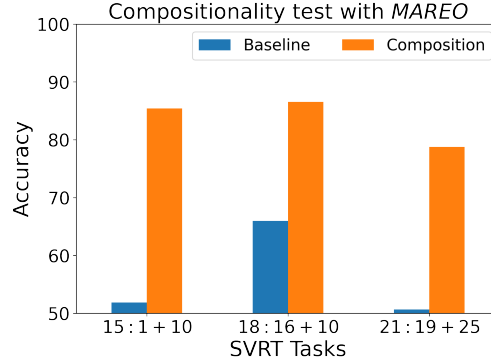


Figure 4: **Compositionality test:** We train the model with tasks containing specific rules (e.g., Task 1 representing same/different discrimination & task 10 involving identification if the four shapes form a square or not). We show that with its ability to compose already learned rules, *MAREO* can quickly learn with 10 samples per class to adapt to a novel scenario (e.g., 15 where the rule is to identify if the four shapes forming a square are identical or not.)

triplets are described in SI section S1.4. We study the ability of the network to learn to compose a new relation with very few training samples, given that it had previously learned the individual rules. We first trained the model with tasks  $x, y$  so that the rules are learned with the help of the reasoning module  $r_\theta$ . The first layer learns the elementary operation over the context vectors stored in the memory block ( $M$ ), and the second layer learns to combine those operations for the tasks  $z$ . We freeze the model after training with tasks  $x, y$  and only fine-tune: (i) a layer to learn to combine elementary operations ( $r_\theta$ ) and (ii) a decision layer ( $f_\phi$ ) on tasks  $z$  with ten samples per category and 100 epochs total. Results are shown in Fig. 4.

## 5 Ablation Study

We now proceed to study what role different components of the proposed architecture play in *MAREO*'s ability to learn reasoning tasks. In our first set of experiments, we selected essential building blocks of the model such as the relational vector ( $all_{obj}$ ), feature channel gain vector ( $g$ ), weighing factor ( $w_{k_t}$ ) at time step  $t$  corresponding to how relevant are the elements stored in memory in order to get the next query, the role of the controller's output ( $out$ ) in the final decision layer ( $f_\phi$ ) and temporal context normalization ( $tcn$ ) on the encoded representation. We studied the effect of these components on SD and SR categories. Our lesioning study revealed that TCN plays a vital role in the model's reasoning capability even for learning simple rules, as in SR tasks. We also found that for SD tasks, excluding  $out$  from the decision-making process is detrimental. Finally,  $g$  and  $w_{k_t}$  have their visible role for tasks containing complex rules (7 Fig. S3). We have summarized the results in Fig. 5a and added additional analyses in SI S1.

In the second part, we evaluated our guided-attention module (*MAREO*) and compared it with self-attention (*MAREO-SA*) and no attention (or memory) (*MAREO w/o Attn (RN)*) variants over 23 SVRT tasks. *MAREO-SA* is similar to ARNe (Hahne et al., 2019) used for solving raven's task. We found that our guided attention module performs 8% better than the SA counterpart and 20% higher than without attention (or memory) for SD tasks, making it computationally efficient while yielding a higher performance (Fig. 5b). ESN (memory-based model) performance on SD tasks in both the visual reasoning dataset shows the importance of attention needed for reasoning. We also plot the saliency maps of the model in Fig. 6 at each time step and show the way in which the model attends to task-dependent features while learning the rules.

## 6 Discussions

Prior cognitive science and active vision literature draw attention to the iterative interaction between perception, memory, and reasoning (Aditya et al., 2016). In an active vision framework, the visual system explores the environment to infer the current task (Fermüller and Aloimonos, 1995). Limiting the part of the scene to be explored significantly reduces the number of computations involved in comprehending it. Experiments (Hayhoe, 2000) on overt visual attention show that eye movement patterns are organized according to task-dependent routines. These routines are sequences of elementary operations needed to complete perceptual tasks involving eye movements and processing foveated scene regions like location storing and contour tracing. Visual routines are a fundamental concept for active vision as it provides the means to select the specific portions of the scene to perform visual processing operations. The operational procedure of our

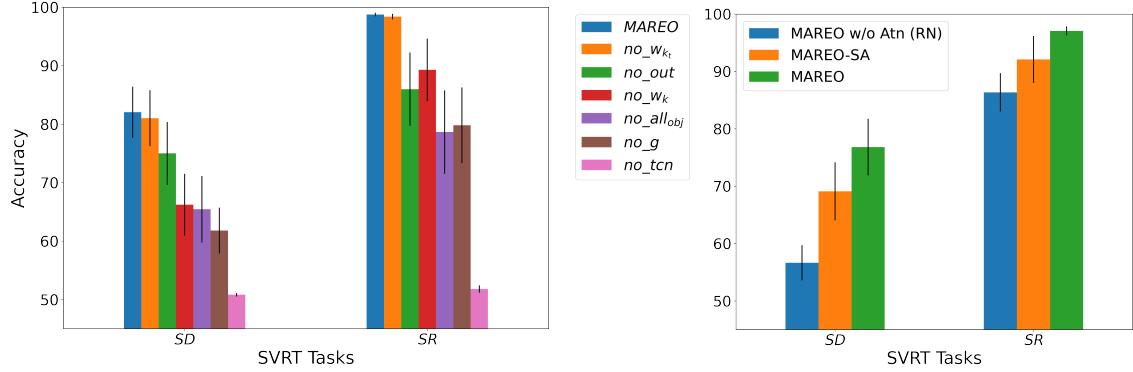


Figure 5: Ablation studies for *MAREO*. (a) We pruned separate parts of the model, one at a time, like the weighting factor at each time step ( $w_{k_t}$ ), controller output ( $out$ ), guided-attention ( $w_k$ ), relational vector ( $all_{obj}$ ), feature channel gain factor ( $g$ ) and temporal context normalization ( $tcn$ ) and show the variation in performance on SD and SR tasks when trained with 1k samples. (b) We also compared the mean accuracy over two sub-clusters of SVRT obtained by *MAREO* with its variant when we replaced the guided-attention module with the self-attention (*MAREO-SA*) and when we completely gave away attention (also memory) and made it a relational reasoning architecture (*MAREO w/o Attn (RN)*).

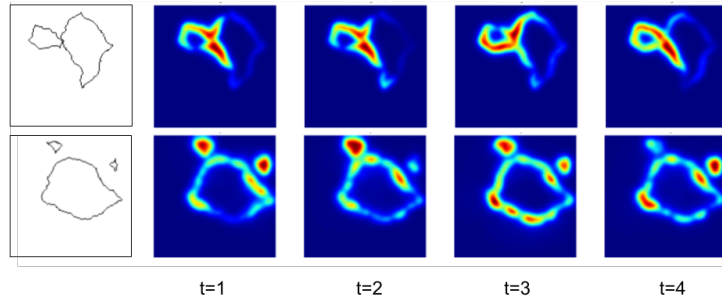


Figure 6: Shift of attention with each time step in a task-dependent manner. In the first row, the task is to answer if the two shapes are touching each other from the outside. At each time step, the network explores the area where the shapes are touching each other. In the second row, tasks represented require to answer if one of the smaller shapes is inside a larger shape. The controller module for this task shifts attention across different shapes at each time step.

model fits well with the long history of cognitive science theory related to this theory of “visual routines”. Influenced by a theory of vision (Marr, 1982), a theoretical framework for visual routine was initially proposed by Ullman (1984). Multiple works indicate that similar mechanisms are taking place in humans (Hayhoe, 2000; Roelfsema et al., 2000; Roelfsema and de Lange, 2016). Despite all the advantages of our model, one of its limitations is that it currently only deals with a fixed number of time steps ( $t=4$ ). Training the model with four time steps was sufficient to capture all the rules available in the SVRT and ART tasks. However, a dynamic method to let the model adapt the number of time steps according to its need should improve the model.

## 7 Related Work

Previous studies (Alamia et al., 2021) have shown that mechanisms associated with attention and memory are involved in solving same-different visual reasoning tasks. Prior work on SVRT studies has focused on the role of attention in solving some of these more challenging tasks. In SVRT, some of the tasks are significantly more challenging for computer vision algorithms than others. In particular, tasks that involve same-different (SD) judgements appear to be significantly harder for neural networks to learn compared to those involving spatial relation judgement (SR) (Stabinger et al., 2016; Yihe et al., 2019; Kim et al., 2018) (see Ricci et al. (2021) for a recent review). Motivated by neuroscience principles, Vaishnav et al. (2022) studied how the addition of feature-based and spatial attention mechanisms differentially affects the learnability of the tasks. These authors found that SVRT tasks could be further taxonomized according to their differential demands for these two types of attention. In another attempt to leverage

a transformer network to incorporate attention mechanisms for visual reasoning, Messina et al. (2021a) proposed a recurrent extension of the classic Vision Transformer block (R-ViT). Spatial attention and feedback connections helped the transformer to learn visual relations better. The authors compared the accuracy of four same-different (SVRT) tasks (tasks *1,5,20,21*) to demonstrate the efficacy of their model. They also showed that, even with 400k samples available for training, neither a Relational Network (Santoro et al., 2017) nor a Vision Transformer (Dosovitskiy et al., 2020) were capable of learning these tasks. While a recent work Webb et al. (2021) has explored the role of memory in visual reasoning tasks.

With the introduction of transformer networks, attention mechanisms started gaining popularity in computer vision. They can either complement (Bello et al., 2019; Vaishnav et al., 2022; d’Ascoli et al., 2021) or completely replace existing CNN architectures (Ramachandran et al., 2019; Touvron et al., 2021; Dosovitskiy et al., 2020). Augmenting the attention networks with the convolution architectures helps them explore the best of both, and they train relatively faster. In contrast, stand-alone attention architecture takes time to develop similar inductive biases as CNN. As initially introduced by Vaswani et al. (2017), transformer attention uses a key (k), query (q), and value (v) attention mechanisms for NLP. Since the images are not like language, all the existing architectures for image recognition explore self-attention variants in which the key, query, and values are the same as an input image. We used a similar attentional system, but instead of using it as a self-attention module, we call it a guided attention module. This system internally generates a query to guide the attention module to the location essential for the task. Since there could be more than one location where the model will attend, we then implemented a memory bank.

We took inspiration for the memory bank from Webb et al. (2021) where mechanisms for variable binding and indirection were introduced in architecture for visual reasoning with the help of external memory. Variable binding is the ability to bind two representations, and indirection is the mechanism involved in retrieving one representation to refer to the other. These authors also introduce Temporal Context Normalization (TCN) (Webb et al., 2020), which is found beneficial for out-of-distribution generalization for relational reasoning tasks. However, the model exhibits significant limitations: It assumes an object-centric image representation whereby objects are presented individually in a sequence. We cannot evaluate such an architecture on the SVRT challenge because images in each task contain multiple objects which require individuation. There are also some relations, like “touching”, which this individuation cannot represent (or any object-centric architecture). ESN also lacks an attentional mechanism and works best in a scenario where hard attention at the pre-processing level helps to simplify the tasks. We tested this template matching behavior of the architecture by training it in the presence of Gaussian noise, and it led to a chance-level performance (refer to SI S7 for more details). Here, we build on this work and describe an end-to-end trainable model that learns to individuate task-relevant scenes and store their representations in memory to allow the judging of complex relations between these objects. Finally, our relational mechanism is inspired by the work in Santoro et al. (2017) that introduced a plug-and-play model for computing relations between object-like representations in a network.

## 8 Conclusion

In this paper, we propose a model *MAREO* to bridge the gap between the reasoning ability of humans and machines. *MAREO*, is a memory and attention base model for reasoning inspired by studies in cognitive science literature. Our model works similarly to how the human brain processes a vast amount of information with the help of selective attention and processing those incremental representations to understand a scene. *MAREO* has the same ability to shift attention actively in a task-dependent manner. In addition to the attention, the two other building blocks in the model are the memory and reasoning modules. A differentiable memory block stores all the elementary representations extracted from a scene, and the reasoning block learns the task-appropriate visual routines over those representations. These features make our model both data and parameter efficient. We demonstrate the model’s versatility, robustness, generalization ability, and compositionality through various experiments, achieving the state of the art results for two visual reasoning challenges. Furthermore, we characterize different strategies (including shortcuts) used by our model with the help of explainability methods and show that the model adapts to the novel tasks and rearranges the elemental processing steps to learn the rules without involving any training. We believe that *MAREO* will also prove to be advantageous for other reasoning challenges.

## Acknowledgments

We want to thank Jonathan D. Cohen (Princeton University), Taylor Webb (UCLA), Minju Jung (Brown University) and Aimen Zerroug (ANITI, Brown University) for helpful discussions. We also want to acknowledge Thomas Fel’s (ANITI, Brown University) help in feature visualization.

This work is funded by NSF (IIS-1912280) and ONR (N00014-19-1-2029) to TS. Additional support was provided by the ANR-3IA Artificial and Natural Intelligence Toulouse Institute (ANR-19-PI3A-0004). Computing resources used supported by the Center for Computation and Visualization (NIH S10OD025181) at Brown and CALMIP supercomputing center (Grant 2016-p20019, 2016-p22041) at Federal University of Toulouse Midi-Pyrénées.

## References

- Aditya, S., Baral, C., Yang, Y., Aloimonos, Y., and Fermuller, C. (2016). Deepiu: An architecture for image understanding. *Advances of Cognitive Systems*.
- Akiba, T., Sano, S., Yanase, T., Ohta, T., and Koyama, M. (2019). Optuna: A next-generation hyperparameter optimization framework. In *Proceedings of the 25rd ACM SIGKDD International Conference on Knowledge Discovery and Data Mining*.
- Alamia, A., Luo, C., Ricci, M., Kim, J., Serre, T., and VanRullen, R. (2021). Differential involvement of eeg oscillatory components in sameness versus spatial-relation visual reasoning tasks. *eNeuro*, 8(1).
- Barrett, D., Hill, F., Santoro, A., Morcos, A., and Lillicrap, T. (2018). Measuring abstract reasoning in neural networks. In *International conference on machine learning*, pages 511–520. PMLR.
- Bello, I., Zoph, B., Vaswani, A., Shlens, J., and Le, Q. V. (2019). Attention augmented convolutional networks. In *Proceedings of the IEEE/CVF international conference on computer vision*, pages 3286–3295.
- Chapman, D. (1992). *Vision, Instruction, and Action*. MIT Press, USA.
- d’Ascoli, S., Touvron, H., Leavitt, M., Morcos, A., Biroli, G., and Sagun, L. (2021). Convit: Improving vision transformers with soft convolutional inductive biases. *arXiv preprint arXiv:2103.10697*.
- Dosovitskiy, A., Beyer, L., Kolesnikov, A., Weissenborn, D., Zhai, X., Unterthiner, T., Dehghani, M., Minderer, M., Heigold, G., Gelly, S., et al. (2020). An image is worth 16x16 words: Transformers for image recognition at scale. *arXiv preprint arXiv:2010.11929*.
- Ellis, K., Solar-Lezama, A., and Tenenbaum, J. B. (2015). Unsupervised learning by program synthesis. In *NIPS*.
- Fermüller, C. and Aloimonos, Y. (1995). Vision and action. *Image and vision computing*, 13(10):725–744.
- Fleuret, F., Li, T., Dubout, C., Wampler, E. K., Yantis, S., and Geman, D. (2011). Comparing machines and humans on a visual categorization test. *Proceedings of the National Academy of Sciences*, 108(43):17621–17625.
- Funke, C. M., Borowski, J., Stosio, K., Brendel, W., Wallis, T. S. A., and Bethge, M. (2021). Five points to check when comparing visual perception in humans and machines. *Journal of Vision*.
- Gentner, D. and Markman, A. B. (1997). Structure mapping in analogy and similarity. *American psychologist*, 52(1):45.
- Hahne, L., Lüddecke, T., Wörgötter, F., and Kappel, D. (2019). Attention on abstract visual reasoning. *arXiv preprint arXiv:1911.05990*.
- Hayhoe, M. (2000). Vision using routines: A functional account of vision. *Visual Cognition*, 7(1-3):43–64.
- He, K., Zhang, X., Ren, S., and Sun, J. (2016). Deep residual learning for image recognition. In *Proceedings of the IEEE conference on computer vision and pattern recognition*, pages 770–778.
- Hu, S., Ma, Y., Liu, X., Wei, Y., and Bai, S. (2020). Hierarchical rule induction network for abstract visual reasoning. *arXiv preprint arXiv:2002.06838*, 2(4).
- Kim, J., Ricci, M., and Serre, T. (2018). Not-so-clevr: learning same–different relations strains feedforward neural networks. *Interface focus*, 8(4):20180011.
- Kingma, D. P. and Ba, J. (2014). Adam: A method for stochastic optimization. *arXiv preprint arXiv:1412.6980*.
- Lovett, A. and Forbus, K. (2017). Modeling visual problem solving as analogical reasoning. *Psychological review*, 124(1):60.
- Maes, P., Darrell, T., Blumberg, B., and Pentland, A. (1994). Alive: Artificial life interactive video environment. In *AAAI*, page 1506.

- Maes, P., Darrell, T., Blumberg, B., and Pentland, A. (1995). The alive system: Full-body interaction with autonomous agents. In *Proceedings Computer Animation'95*, pages 11–18. IEEE.
- Marr, D. (1982). *Vision: A Computational Investigation into the Human Representation and Processing of Visual Information*. Henry Holt and Co., Inc., USA.
- Messina, N., Amato, G., Carrara, F., Gennaro, C., and Falchi, F. (2021a). Recurrent vision transformer for solving visual reasoning problems. *arXiv preprint arXiv:2111.14576*.
- Messina, N., Amato, G., Carrara, F., Gennaro, C., and Falchi, F. (2021b). Solving the same-different task with convolutional neural networks. *Pattern Recognition Letters*, 143:75–80.
- Michal, A. L. and Franconeri, S. L. (2017). Visual routines are associated with specific graph interpretations. *Cognitive research: principles and implications*, 2(1):1–10.
- Puebla, G. and Bowers, J. S. (2021). Can deep convolutional neural networks learn same-different relations? *bioRxiv*.
- Ramachandran, P., Parmar, N., Vaswani, A., Bello, I., Levskaya, A., and Shlens, J. (2019). Stand-alone self-attention in vision models. *arXiv preprint arXiv:1906.05909*.
- Ramachandran, V. S. (1985). Apparent motion of subjective surfaces. *Perception*, 14(2):127–134.
- Ricci, M., Cadène, R., and Serre, T. (2021). Same-different conceptualization: a machine vision perspective. *Current Opinion in Behavioral Sciences*, 37:47 – 55.
- Roelfsema, P. R. and de Lange, F. P. (2016). Early visual cortex as a multiscale cognitive blackboard. *Annual review of vision science*, 2:131–151.
- Roelfsema, P. R., Lamme, V. A., and Spekreijse, H. (2000). The implementation of visual routines. *Vision Research*, 40(10):1385–1411.
- Santoro, A., Raposo, D., Barrett, D. G., Malinowski, M., Pascanu, R., Battaglia, P., and Lillicrap, T. (2017). A simple neural network module for relational reasoning. *arXiv preprint arXiv:1706.01427*.
- Simonyan, K., Vedaldi, A., and Zisserman, A. (2014). Deep inside convolutional networks: Visualising image classification models and saliency maps. In *In Workshop at International Conference on Learning Representations*. Citeseer.
- Smilkov, D., Thorat, N., Kim, B., Viégas, F., and Wattenberg, M. (2017). Smoothgrad: removing noise by adding noise. *arXiv preprint arXiv:1706.03825*.
- Spratley, S., Ehinger, K., and Miller, T. (2020). A closer look at generalisation in raven. In *European Conference on Computer Vision*, pages 601–616. Springer.
- Stabinger, S., Peer, D., Piater, J., and Rodríguez-Sánchez, A. (2021). Evaluating the progress of deep learning for visual relational concepts. *Journal of Vision*, 21(11):8–8.
- Stabinger, S., Rodríguez-Sánchez, A., and Piater, J. (2016). 25 years of cnns: Can we compare to human abstraction capabilities? In *International Conference on Artificial Neural Networks*, pages 380–387. Springer.
- Sundararajan, M., Taly, A., and Yan, Q. (2017). Axiomatic attribution for deep networks. In *International Conference on Machine Learning*, pages 3319–3328. PMLR.
- Touvron, H., Cord, M., Douze, M., Massa, F., Sablayrolles, A., and Jegou, H. (2021). Training data-efficient image transformers and distillation through attention. In *International Conference on Machine Learning*, volume 139, pages 10347–10357.
- Tsotsos, J. K. (1990). Analyzing vision at the complexity level. *Behavioral and brain sciences*, 13(3):423–445.
- Ullman, S. (1984). Visual routines. *Cognition*, 18:97–159.
- Ullman, S. (1987). Visual routines. In *Readings in computer vision*, pages 298–328. Elsevier.
- Vaishnav, M., Cadene, R., Alamia, A., Linsley, D., VanRullen, R., and Serre, T. (2022). Understanding the Computational Demands Underlying Visual Reasoning. *Neural Computation*, pages 1–25.

- Vaswani, A., Shazeer, N., Parmar, N., Uszkoreit, J., Jones, L., Gomez, A. N., Kaiser, Ł., and Polosukhin, I. (2017). Attention is all you need. In *Advances in neural information processing systems*, pages 5998–6008.
- Webb, T., Dulberg, Z., Frankland, S., Petrov, A., O’Reilly, R., and Cohen, J. (2020). Learning representations that support extrapolation. In *International Conference on Machine Learning*, pages 10136–10146. PMLR.
- Webb, T. W., Sinha, I., and Cohen, J. D. (2021). Emergent symbols through binding in external memory. *ArXiv*, abs/2012.14601.
- Yihe, L., Lowe, S. C., Lewis, P. A., and van Rossum, M. C. W. (2019). Program synthesis performance constrained by non-linear spatial relations in synthetic visual reasoning test. *ArXiv*, abs/1911.07721.
- Yu, Z., Yu, J., Cui, Y., Tao, D., and Tian, Q. (2019). Deep modular co-attention networks for visual question answering. In *Proceedings of the IEEE Conference on Computer Vision and Pattern Recognition (CVPR)*, pages 6281–6290.
- Zhang, C., Gao, F., Jia, B., Zhu, Y., and Zhu, S.-C. (2019). Raven: A dataset for relational and analogical visual reasoning. In *Proceedings of the IEEE Conference on Computer Vision and Pattern Recognition (CVPR)*.

# Supplementary Information

## S1 In depth analysis of MAREO

To better understand the architecture of MAREO, we describe the algorithm in 1.

**Algorithm 1** Memory and Attention-based visual REasOning model (MAREO). ( $\parallel$ ) indicates the concatenation of two vectors, forming a new vector.  $\{, \}$  indicates the concatenation of a matrix and a vector, forming a matrix with one additional row.

---

```

 $k_{r_{t=1}} \leftarrow 0$ 
 $h_{t=1} \leftarrow 0$ 
 $M_{t=1} \leftarrow \{\}$ 
 $z_{img} \leftarrow f_e(x_{in})$  ▷ base representation
for  $t$  in  $1 \dots T$  do
   $out, g, query_t, h_t \leftarrow f_s(h_{t-1}, k_{r_{t-1}})$ 
   $w_k \leftarrow (guided\ attention(z_{img}, query_t)).sum(axis = 1)$  ▷ attention module
   $z_t \leftarrow (z_{img} * w_k).sum(axis = 1)$  ▷ elemental representation
  if  $t$  is 1 then
     $k_{r_t} \leftarrow 0$ 
  else
     $w_{k_t} \leftarrow w_k.sum(axis = 2)$ 
     $k_{r_t} \leftarrow g * (M_{t-1} * w_{k_t})$ 
  end if
   $M_t \leftarrow \{M_{t-1}, z_t\}$ 
end for
 $all_{obj} \leftarrow r_\theta(\sum_{i,j=1}^T (M_{v_i}, M_{v_j}))$  ▷ reasoning module
 $\hat{y} \leftarrow f_\phi(all_{obj} \parallel out)$ 

```

---

### S1.1 Guided Attention

Transformer (Vaswani et al., 2017) architectures used self-attention mechanisms to draw global dependencies between input and output. In self-attention, input interacts with itself to estimate where more attention has to be paid with the help of key, query and value dot product. Self-attention is composed of three steps (i) dot product similarity score, (ii) normalizing scores to obtain weights, and (iii) re-weighting the original embeddings using weights.

$$self\ attention = softmax\left(\frac{QK^T}{\sqrt{d}}\right)V$$

where ‘d’ is the dimension of  $K$  and  $V$ . To calculate the  $Q$ ,  $K$  and  $V$  from an input  $X$ , there are trainable weight matrices  $W_q$ ,  $W_k$  and  $W_v$ .

$$\begin{aligned} Q &= XW_q \\ K &= XW_k \\ V &= XW_v \end{aligned}$$

However, in *guided-attention*, we take query as  $z_{img}$ , key and value vectors as  $query_t$  from the controller without any trainable matrix. So the attention score becomes

$$guided\ attention\ (GA) = softmax\left(\frac{z_{img} \cdot query_t^T}{\sqrt{128}}\right)query_t$$

as the dimensionality of the vector is  $\mathcal{R}^{128}$ . This guided-attention ( $GA \in \mathcal{R}^{hw \times 128}$ ) score is summed across the spatial dimension ( $h \times w$ ) to re-weight the feature channels of the  $z_{img}$  and form  $z_t$  vector. This module acts like a feature-based attention module because of its ability to modulate the channels and only store the feature vector in the memory. We also illustrated the multi-head attention in Figure S1.

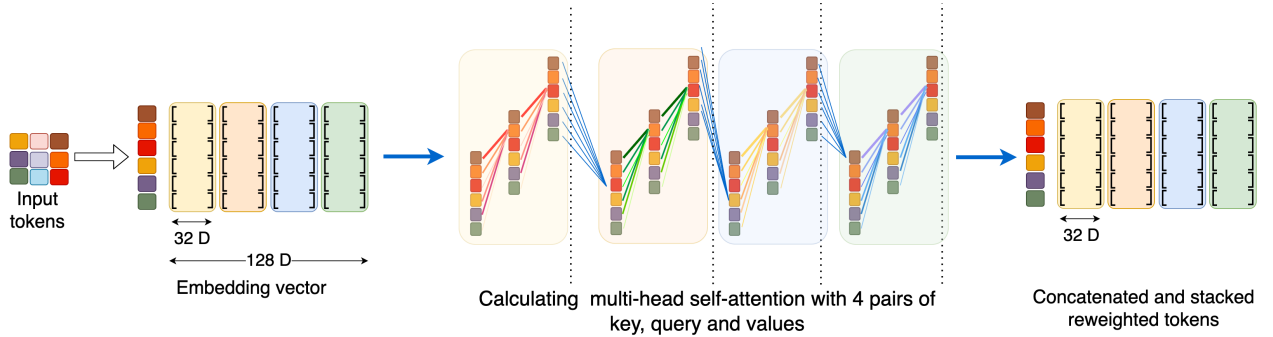


Figure S1: Multi-Head Attention in an image. After the encoder module, the image is flattened, where each spatial dimension is taken as a token. As the spatial dimension is  $8 \times 8$ , there are 64 tokens. In 4-headed attention, a 128-dimensional feature vector is divided into 32-D vectors, and each head focuses on finding the association particular token with the others, which are concatenated back to 128-D.

**Characterizing the learned strategies with explainability methods** We used three attribution methods: *Integrated-gradients* (Sundararajan et al., 2017), *Saliency* (Simonyan et al., 2014) and *SmoothGrad* (Smilkov et al., 2017). Common to these methods is the use of the gradient of the classification units w.r.t. the input image. These methods help characterize the visual features that are diagnostic for the network prediction (e.g., SI section S3).

## S1.2 Learning rules

**Rules involving Same-Different (SD) identification** In task 1, the challenge is to differentiate between the two shapes and recognize if these two shapes are the same or different. When we trained the model on task 1, it (1) learned a mechanism to attend to the two shapes presented in an image; (2) learned to judge the similarity between the two shapes. To test the models’ generalization ability, we selected tasks demanding similar judgment to decide. There are three of those from the set of 23 satisfying this criterion, 5, 15 and 22. In task 15, four shapes form a square; in category 1, all these shapes are identical. Compositions involved in this task are identifying the same shape and counting them to make a correct decision. *MAREO* has shown its ability to attend to all the identical shapes (Fig. S13) and make a correct decision with 92.53% accuracy. The model learns a similar ability when trained with task 21. It has two shapes that are rotation, scaled, or translated form. The reason task 21 could solve task 15 is same as before with 1.

In task 22, there are three shapes aligned in a row. All of them are identical in category 1. Again, the model must count the number of identical shapes and take the correct decision if the count reaches 3. In this task, our model achieves 84.91% accuracy. Another task taking the decision based on counting is 5. The model needs to identify if two pairs of identical shapes are present in the image. However, when we evaluate ResNet-50 on these three tasks, we believe that the model must have found a shortcut to make a decision. ResNet-50 has learned a strategy to count only one pair of identical shapes, and it takes the decision as soon as it finds that identical pair in tasks 5, 15, 22 and performs better than chance level.

Next, we try to understand the learning of the model trained on task 5. The model trained with 5 has learned to identify the two pairs of identical shapes from a group of four. We found that the network is exploring a shortcut to solve this task. Rather than learning to find both pairs of identical shapes, it learned to attend to only one pair to take a judgment (Fig. S7). Still, the model’s routine helps extend this mechanism and attend to more than two shapes if shown in the same stimulus. At the same time, R50 uses its template matching technique to explore one pair of identical shapes, which helps it to solve task 1 but does not help on tasks 15 and 22.

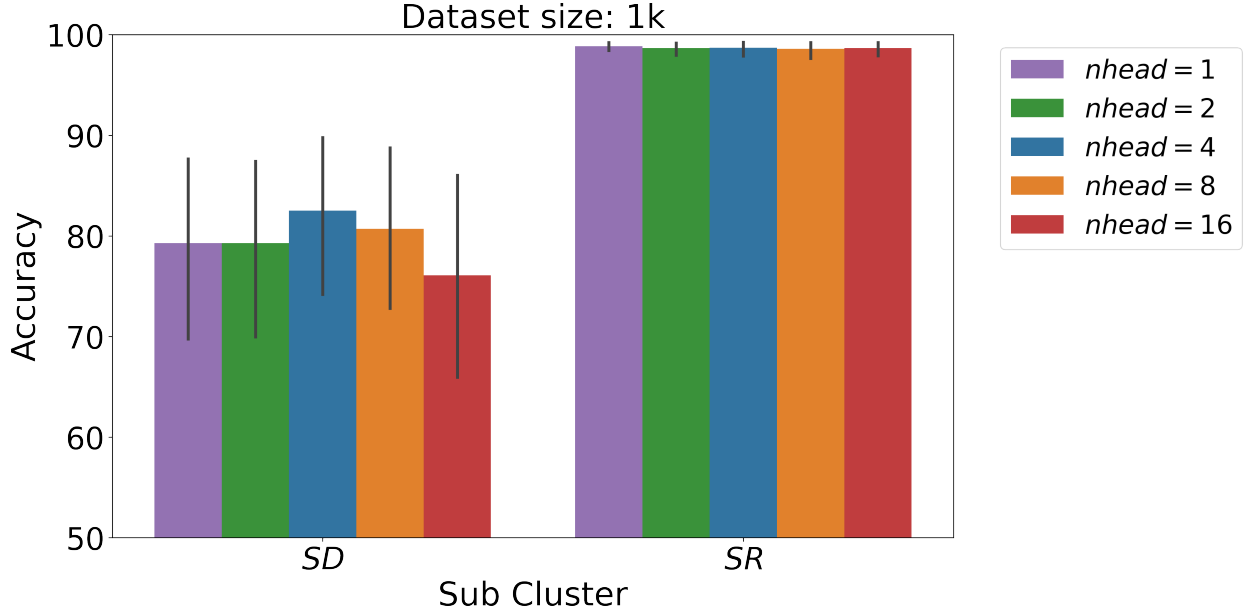


Figure S2: Ablation on Multi-Head Attention. We analyzed the average performance on SVRT tasks by changing the number of heads ( $1, 2, 4, 8, 16$ ) and 1k images used for training. On average, this effect is distinguishable in *SD* tasks while *SR* tasks are already at their ceiling. The embedding dimension of each head is consistent with the defacto transformer architecture where the embedding dimension is 512-D and 16 heads i.e. 32-D vector for each head.

In task 7, the model learns to identify and count identical shapes in an image. There are three pairs of two identical shapes vs. two pairs of three identical shapes, as seen in Fig. S7. We test this model on task 22 and obtained 83.8% accuracy. Here the rule is to identify if three identical shapes form a row or not. However, a model trained on task 22 cannot solve task 7 because it explores a shortcut in solving task 22. It compares two shapes and arrives at a decision (Fig. S8) whereas, in task 7, grouping and counting are required to make a decision. R50, on the other hand, might still be looking for only one pair of identical shapes (there are three pairs in total) to make a decision. Thus fail to adapt to a novel task.

**Rules involving Spatial Relations** In addition to solving *SD* tasks, we show that *MAREO* also learns the routines when the judgment requires spatial reasoning. In tasks 11 and 2, the challenge is to inspect if the two shapes are touching/around the corner or not. One of the smaller shapes in these tasks is towards the boundary from inside (task 2) or touching from outside (task 11). Training one and testing the other yields  $> 95\%$  accuracy. In Fig. S16 we can see from the attribution maps that the model is focusing on the area where the two shapes are touching to reach a decision. In task 23, the challenge is to learn insiderness. Task 23 has two small and one large shape; both the small shapes are either inside or outside in one category vs. one shape inside and one outside in category 2. We test the model on task 8, which has two shapes, one inside the other and identical in one category vs. outside in category 2. When we train a model on task 23, it learns the judgment of insiderness and also counts the number of shapes present inside. If we evaluate such a model on task 8, it quickly figures out instances when the shape is inside or outside (probably not identical).

For all these experiments, we take 10k samples for training the network for tasks 1, 5, 7, 21, 23, 11, 2 and then perform the zero-shot generalization on a novel set of tasks.

### S1.3 Reverse Curriculum

In this part of the experiment, we go beyond making a decision based on the learned rule and analyze *MAREO*'s ability to parse those rules individually and evaluate tasks containing simpler rules. We trained *MAREO* on a complex task and tested it on its elementary subset. For example, in task 19, the rules involved are to learn the scale invariance between two shapes in a stimulus. After training the model on task 19, we tested for the case where the scale factor is 1 (not seen during training), i.e., task 1, and obtained 94.05% accuracy. Similarly, we took another task 21, where there are two

elementary operations involved, scaling and rotation together (non zero values). To see if *MAREO* has the ability to parse this complex relation we tested the model trained on task 21 on task 19 (scaling =  $x$  and rotation = 0) and task 1 (scaling = 1 and rotation = 0) and obtain 86.95% and 90.86% respectively. It shows *MAREO*'s unique ability to parse a complex set of relations into independent simple elementary unseen relations.

#### S1.4 Learning Composition

We selected group corresponding to each tasks (15, 18, 21) used for composition. Task 15 has four shapes which are forming a square and are also identical. It can be composed of task 1 helping to identify the same shapes and task 10 which helps to learn if the four shapes are forming a square. In task 18, a rule is needed to be learned related to symmetry along the perpendicular bisector of the image. It can be taken as a composition of task 16 which requires learning mirror reflection of the image along the perpendicular bisector of the image and task 10 where in which symmetry could be discovered in between 4 shapes (forming a square). At last, we took task 21 which involves both scaling and rotation between two shapes in an image. As its compositional elements, we designed a variant where there is only rotation and no scaling and represented it with 25 and combined it with another counterpart of 21 where there is scaling and no rotation, i.e., task 19.

#### S1.5 Ablation Study

As different SVRT tasks vary in terms of complexity, we studied the effect of these components on a subset of representative tasks instead of averaging over all task complexities. We performed our quantitative analysis with a model trained on 1,000 samples on four different tasks (1, 5, 7, 2). These are selected based on the factors like rules involved in their formulation, reasonable accuracy (when trained with 1k samples), and a representative from both *SD* or *SR* categories.

Overall, we found that the weighting factor at each time step ( $w_{k_t}$ ) has an insignificant drop in the overall performance. Still, we made a place for this variable in the final architecture to further investigate its effect on more complex tasks. However, guided attention ( $w_k$ ) has a substantial role in learning the correct rule.

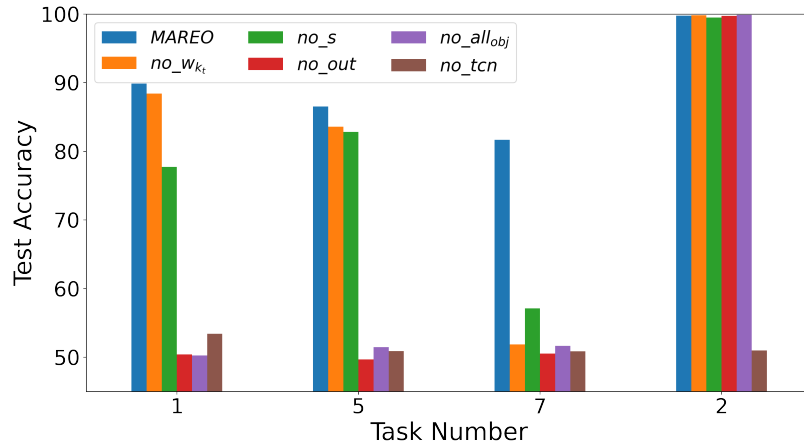


Figure S3: Ablation studies for *MAREO*. (a) We pruned separate parts of the model, one at a time, like the weighting factor at each time step ( $w_{k_t}$ ), feature channel gain factor ( $g$ ), controller output ( $out$ ), relational vector ( $all_{obj}$ ) and temporal context normalization ( $tcn$ ) and show the variation in performance on tasks 1, 5, 7 and 2 when trained with 1k samples.

#### S1.6 Abstract Variable

As seen in our ablation study (section 5), one of the fundamental components responsible for the learning complex rules is *out*, and abstaining from it makes the model struggle. We did a t-SNE analysis on this variable using the first 20 principal components from its 512-dimensional vector as these components contribute to 95% of the variance. We analyzed 200 samples from each task of a class balanced validation dataset. None of these were included in the training.

These components encode the abstract variable for each task and have separable boundaries from each other, as seen in Fig. S4.

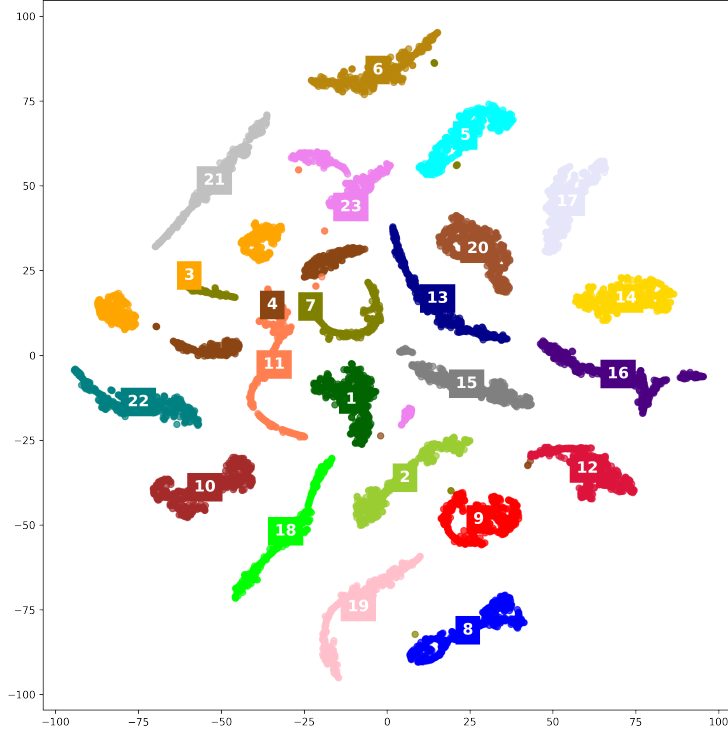


Figure S4: t-SNE plot of the first 20 components of the abstract variable (*out*) obtained via PCA for all 23 SVRT tasks. Those components have a cumulative variance of 95%. Each cluster can be clearly identified from other clusters representing different relations learned. Tasks are represented as labels with the same colored box around them placed in the mean location of the cluster.

### S1.7 Robustness

We did a study to inspect the robustness of the model. We evaluated the model on two factors: robustness to scale and robustness to the noise. We found that *MAREO* is able to extract the correct rules in both these scenarios.

**Scale** We analyzed the performance of the model with changing scale. We train the model with images of resolution  $128 \times 128$  and test them at scale 1.5 times the original, i.e.,  $192 \times 192$ . We found that the model can generalize at this scale to various tasks such as 1, 9, 11, 14, 15, 17. In Table S1, we compared the performances of the model trained on tasks at scale ( $s=1$ ) and tested on task with  $s=1$  with tested on task with  $s=1.5$  for two different training sets, 5k and 10k. We did not use any augmentation relating to changing scale during the training, which might push the model to learn such scale-invariant representations.

In Fig. S5, we demonstrate an example of task 1 highlighting the region considered for taking decision at  $s=1.5$ .

**Noise** We even checked the robustness of *MAREO* to noise. We added Gaussian white noise to the dataset to perform this experiment with 0 mean and .05 variance. We found a negligible difference in the test accuracy of the model with noise when compared to the case without any noise (Fig. S26, S27). We even went further to change the type of the noise to salt and pepper while testing the same model. Nevertheless, the model learned the rules delivering nearly the same test accuracy as before.

## S2 Visual Routines

Every instant vast amount of visual information is presented to the sensory systems in the brain, where it extracts the relevant information. This ability to visually detect, recognize, search or obtain descriptions from the scene helps

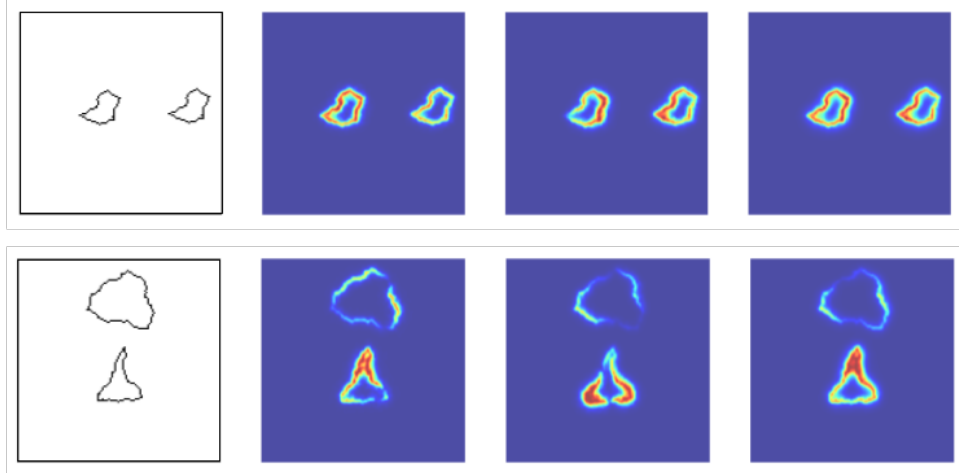


Figure S5: Scale invariance shown by *MAREO* when it is trained with images of dimension  $128 \times 128$  and tested on images of dimension  $192 \times 192$  for task 1. Attribution map shows that when two same shapes are present in an image, the model still tries to compare each part of both the shapes vs when two different shapes are present, it focuses its attention on the most salient part i.e. corners. We show maps from three different attribution methods, Integrated Gradients, Saliency and SmoothGrad.

Table S1: Test accuracies when the model is trained on tasks at scale ( $s$ ) = 1 with 10k and 5k samples and tested on the same tasks at scale ( $s$ ) = 1.5 without any finetuning.

TRAINING TASKS	TEST ACCURACY			
	5K SAMPLES		10K SAMPLES	
	s=1	s=1.5	s=1	s=1.5
1	94.77	71.01	97.34	75.09
9	99.00	70.46	99.58	72.11
11	99.85	90.89	99.75	91.05
14	98.66	71.84	99.62	73.45
15	98.76	73.02	98.59	68.66
17	93.09	72.98	95.13	74.98

us execute various daily life tasks. Studies have also shown the insensitivity to changes in the visual scenes during eye movement, also called "changing blindness." This phenomenon indicates that a scene is represented with only a small amount of available information. For doing this, some mechanism should exist in order to select the relevant information based on the current circumstances.

Despite the complexities of these tasks, the underlying principles of visual processing in the brain are relatively simple. For example, even if the visual system has the capability to analyze curves and contours, it is impossible to represent all the possible combinations of these just by using feature detectors (Ullman, 1984). A similar problem is posed in the visual search scenario. Due to the combinatorial explosion of possible features involved in the formation of a scene, the feedforward detection mechanism finds it hard to understand (Tsotsos, 1990). It shows us that mechanisms exist in our visual system other than simple feature detectors that aid in solving such tasks from the versatility of possible scenes.

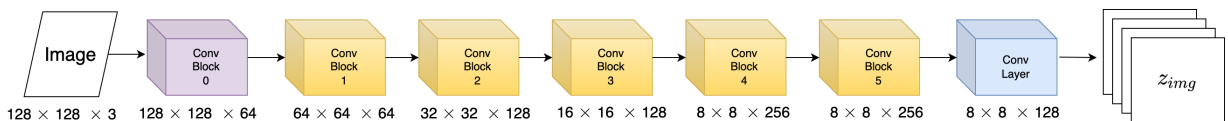


Figure S6: Encoder module ( $f_e$ ) of *MAREO*

To implement such task-dependent visual processing, (Ullman, 1984, 1987) proposed visual routines theory. It is one such method to process visual information beyond creating representations, thereby helping in tasks like object recognition, manipulation and abstract reasoning. A primitive set of operations are defined in Ullman (1987) that are applied to obtain relevant information and spatial relations from a scene. Such a composition of operations is called a *routine*.

The visual routine theory is heavily influenced by the theory of vision by Marr (1982). Ullman and Marr focussed on extensive analysis and used a functional approach as a starting point. This type of analysis provides a framework that, on the one hand, can be used in the theory of human cognition while, on the other hand, equally applicable in designing computer vision systems. This theory is based on similar principles that visual systems can solve tasks that feedforward feature detectors could not do. Tasks are solved with the help of some mechanisms applied on top of these representations obtained by feature detectors (known as base representations). Ullman showed that a model could solve complex tasks if a finite set of simple operations helping the model to reason are sequenced properly (forming a routine). Another similar idea was presented in a utilitarian theory of perception (Ramachandran, 1985). This theory mentions that perception is similar to various parts of the human body, which are collections of ad-hoc pieces, working in their own way as well as together.

Another piece of evidence presented by Roelfsema et al. (2000) showed how the elemental operations required for routines are implemented in the brain. When an image is presented, feedforward processes in the brain lead to the activity pattern distributed across visual areas. Afterward, the elemental operation comes into play as firing rate modulations. These modulations enforce the grouping of neural responses into coherent object representations. Later, Hayhoe (2000) discussed evidence of routine in vision, indicating that only a small part of the information of a scene is represented in a brain at each moment.

A cognitive blackboard theory is postulated in Roelfsema and de Lange (2016), explaining how the activity of neurons in the early visual cortex helps infer the visual world. The writing operations on the blackboard are compared to the feedback signals from higher cortical areas in the early visual cortex. These feedback signals are read by cortical regions and subcortical structures in later processing steps, thereby supporting an exchange of intermediate computational steps.

### S2.1 Relating visual routine theory with *MAREO*:

Visual processing by Ullman can be divided into three stages. First is the creation of *base representation*. It is a bottom-up process in which base representations are generated from the visual input. Once these representations are constructed, a visual processor is used to apply sequences of elemental operations to them in the second step. It extracts the desired information from the base representations in a top-down manner. In the third stage, this extracted information is used to reason in any given task. In humans, the bottom-up process corresponds to the retinotopic maps to capture properties like edge, color, speed and direction of motion. These base representations are dependent on a fixed set of operations uniformly applied over the entire input without any object/task-specific knowledge.

Such sequences of operations to extract information from the base representations are known as *visual routines*. These elemental operations are task-specific that are used to create *incremental representations* containing information to be used in the next operation. Thus, by applying these routines, incremental representations are constructed using sequences of elemental operations, which are finally used to provide a solution particular to the task. Some examples of these elemental operations are as follows: shifting the processing focus, indexing, marking an object or location for future reference, tracing boundaries, and spreading activation over an area delimited by boundaries. In the shift of processing focus, the spotlight of selective attention helps to shift the processing focus on the image from one part to the other. Indexing enlists all locations where processing focus can shift. Routines are generally generated in response to some internally generated queries by assembly mechanisms in response to some specific goals.

Aligned with this theory, our proposed model has different building blocks. These are, base representations ( $z_{img}$ ), incremental representations ( $z_t$ ), memory block to save these incremental representations ( $M$ ), guided attention and finally reasoning module ( $r_\theta$ ). In our model, *base representation* ( $z_{img}$ ) is created using a convolutional encoder ( $f_e$ ) which is a pure bottom-up process. This representation is fixed and calculated using a feedforward network for any particular input.  $z_{img}$  is used to create an incremental representation ( $z_t$ ) using a visual routine processor represented by our guided attention module. At each time step, the guided attention module takes the input as the base representation ( $z_{img}$ ) and query vector coming from a recurrent module ( $f_s$ ). This guided attention module gives the desired task-relevant feature vector to create  $z_t$ , which is stored in the memory bank ( $M$ ) and later used for reasoning.

### S3 Attribution map visualization

Figure S7: Attribution map visualization for SVRT tasks. The map represents the area of the image, which are significant in decision making for *MAREO*. Tasks represented are from 1 to 8. We used three different attribution methods here Integrated Gradients, Saliency and SmoothGrad.

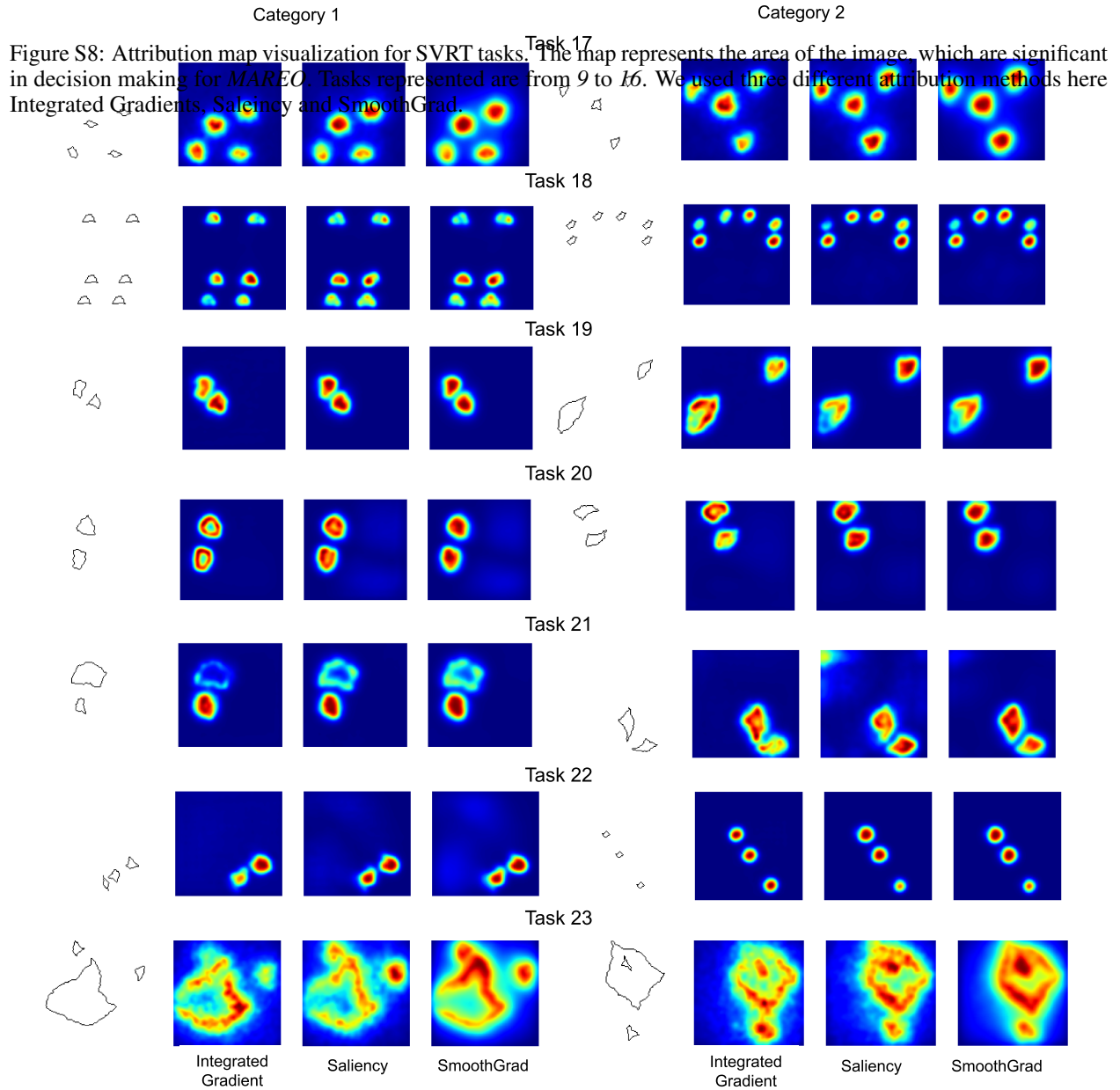


Figure S9: Attribution map visualization for SVRT tasks. The map represents the area of the image, which are significant in decision making for *MAREO*. Tasks represented are from 17 to 23. We used three different attribution methods here Integrated Gradients, Saliency and SmoothGrad.

## S4 Explanation of routines learned and corresponding attribution maps

This section explains the different mechanisms our model learns when we train it with a task and shows how it uses those learning mechanisms to understand the rule while testing on a novel set of tasks.

In Fig. S10, we see the explainability maps corresponding to the model trained with tasks 5, 19, 20 & 21 and we test those models on task 1. Fig. S7 shows that in task 5, the model learned a shortcut to select only one identical pair from a group of two pairs to take a decision. The model learns this shortcut because it was sufficient to make the correct decision. At the same time, to decide on images from category 2, the model stops searching as soon as it finds a non-identical region between two shapes.

In task 19, the model learns scale-invariance. The model chooses one shape and examines a similar part around the second shape to check the scale-invariant representation. A broader version of transformations is learned in task 21, where the model understands rotation, scaling, and translation concurrently. So the model uniformly attends to the two shapes present in the image and compares them.

In task 20, the model learns one of the three types of similarity transformation, i.e., reflection. If a model learns to distinguish similarity, it can solve any reasoning tasks associated with same-different identification.

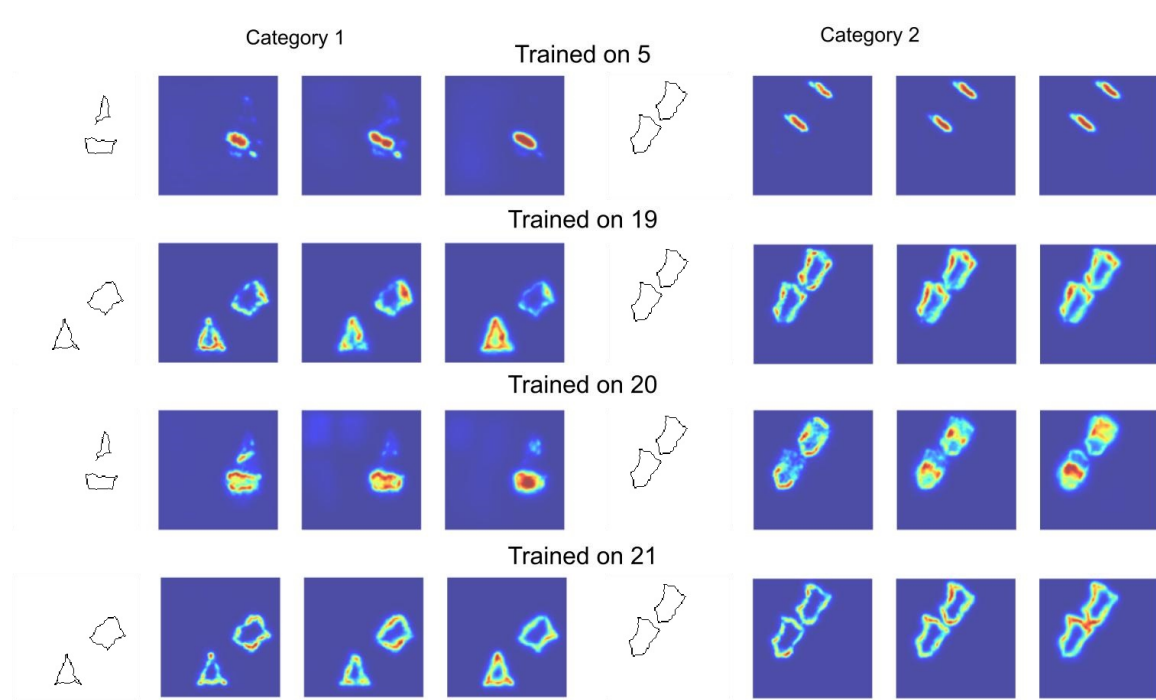


Figure S10: Attribution maps corresponding to the mechanisms involved in visual routines when testing on images from task 1 and the model is trained on different tasks as mentioned above each example image from both the category.

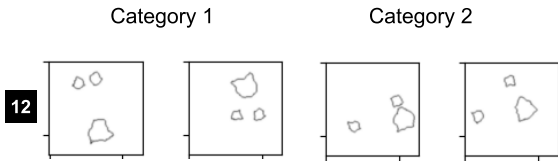
Moving on to Fig. S11, we test the rules learned by tasks 1, 7 & 20 and test on task 22 where the challenge is to identify if the three shapes arranged in a row are identical or not. As seen from the previous discussions, task 1 learns to identify if two shapes are the same or not. As there are three shapes existing, the model tries to compare two shapes in pairs before deciding. So we can see the high heat map values on the two shapes for both tasks. As discussed before, task 20 learned a similarity transformation between two shapes, and it makes a pairwise comparison between three shapes to take a decision.

Glancing at the performance of task 7 on task 22, we claim the model learned to compare the shapes as well as count them to make a decision. Similar to category 2 of task 7, here again, we have three shapes responsible for such a good performance.

Next, we look at the strategy used to solve task 15 in Fig. S13. The rule to formulate the task involved identifying if the four shapes required to form a square are identical. The model trained on task 1, 5, 21 and 22 starts by picking up one

shape and stop comparing when it comes to the fourth shape. This is the reason all of the four shapes in category 2, which are similar, are seen to be involved in decision-making.

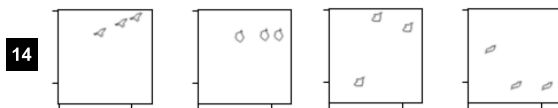
## S5 Example SVRT tasks



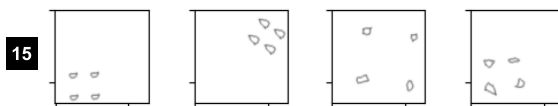
12 Each image contains three different shapes, two of which are the same size. In category 1 the two small shapes are closer together than either one is from the larger shape.



13 Each image contains an identical pair of small shapes and an identical pair of large shapes. In category 1, the four shapes can be grouped into two meta-shapes or compositions, each consisting of one small shape and one large shape with the property that the two resulting compositions are equivalent, i.e., one composition can be translated to become identical to the other.



14 Each image contains three shapes of identical size and shape. In category 1 the three shapes are aligned.



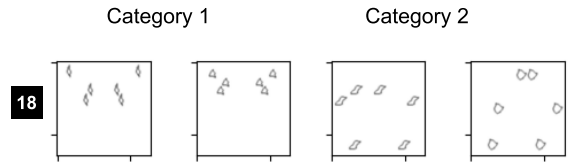
15 Each image contains four equally-sized shapes arranged on the vertices of a square. In category 1 the four shapes are identical.



16 Each image contains six identical shapes. In category 1 one cluster of three shapes can be obtained from the other cluster of three shapes by reflection around the vertical bisector of the image.



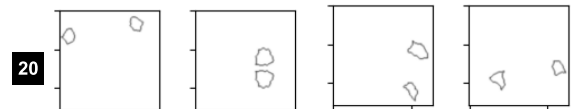
17 Each image contains four shapes, three of which are identical. In category 1, each shape among the identical ones is the same distance from the non-identical one.



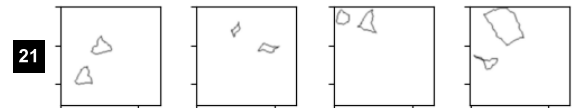
18 Each image contains six identical shapes. In category 1 they are organized into three pairs such that the two shapes in each pair are positioned symmetrically with respect to the vertical bisector of the image.



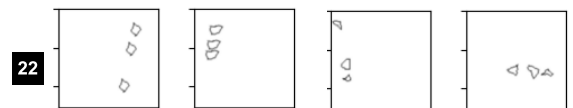
19 Each image contains two shapes of different sizes. In category 1, the two shapes are equivalent up to scaling and translation.



20 Each image contains two shapes. In category 1 one shape can be obtained from the other by reflection around the perpendicular bisector of the line joining their centers.



21 Each image contains two shapes. One of the shapes in category 1 can be obtained from the other by scaling, translating and rotating.



22 Each image contains three aligned shapes. In category 1 the three shapes are identical.



23 Each image contains one large and two small shapes. In category 1, the small shapes are either both inside or both outside the large shape.

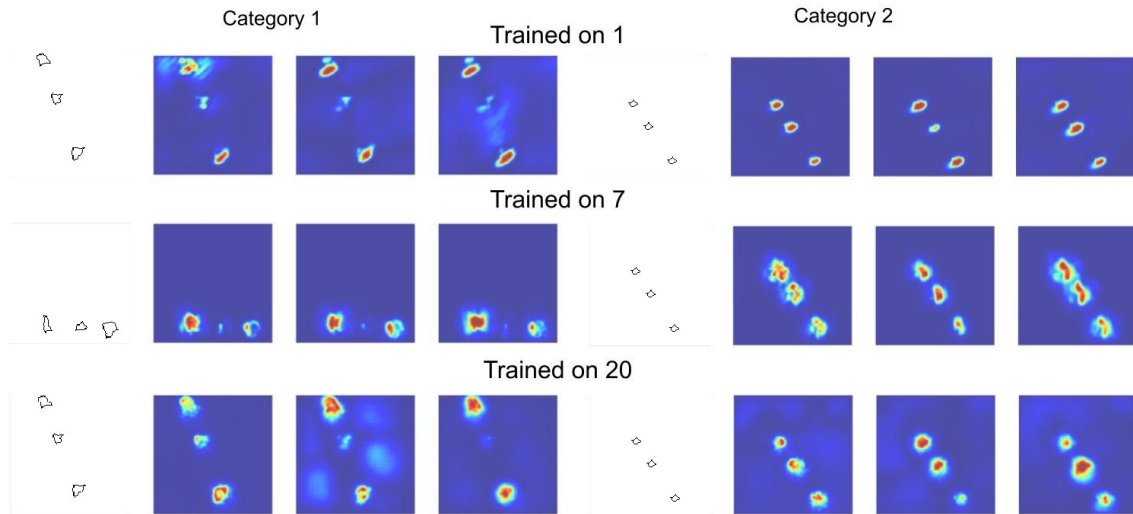


Figure S11: Attribution maps corresponding to the mechanisms involved in visual routines when testing on images from task 22, and the model is trained on different tasks as mentioned above each example image from both the category.



Figure S12: Attribution maps corresponding to the mechanisms involved when training a model on task 23 and testing on images from task 4. One of the rules learned in task 23 is to see if a smaller shape exist inside the large shape, which is the same rule to be tested in category 2 of task 4.

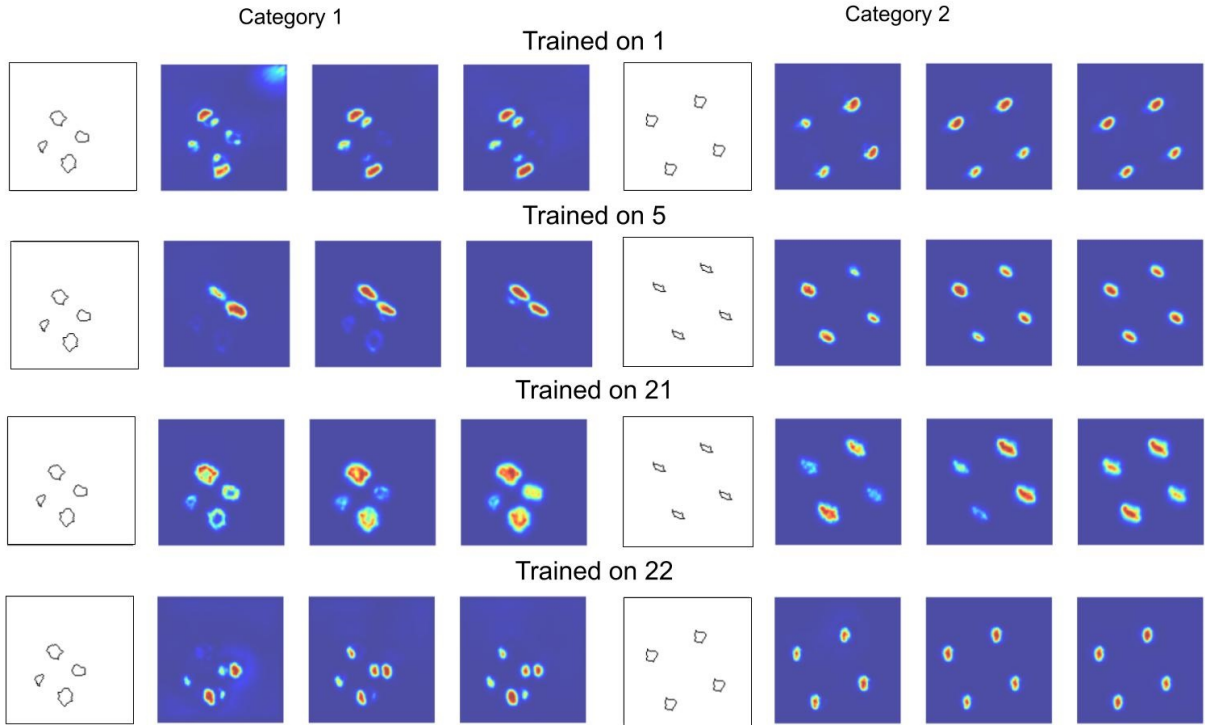


Figure S13: We show the visual routines learned by *MAREO* when training the model on task *1*, *5*, *21*, *22* and we test the same model on task *15* (four shapes forming a square). It shows that once the model has learned to recognize one pair of identical shapes, it can extend the ability to count all the identical shapes present in an image. The visualization shows the attribution methods Integrated Gradients, Saliency, and SmoothGrad from left to right.

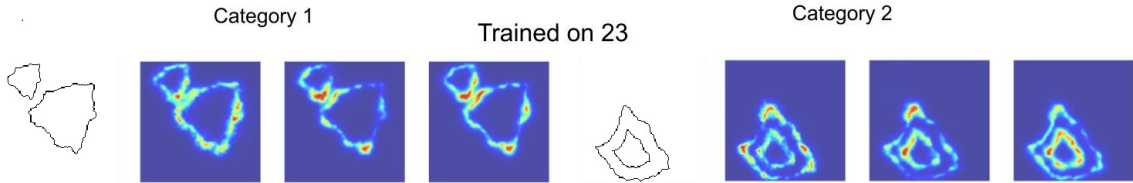


Figure S14: Attribution maps corresponding to the mechanisms learned when training a model on task *23* and testing on task *8*. One of the rules learned in task *23* is to comprehend if one small shape exists inside the large shape. A somewhat similar rule involved in task *8* is to identify if the smaller shape existing inside is also identical or not. The model is probably only answering on the bases of insiderness without considering same-different judgement.

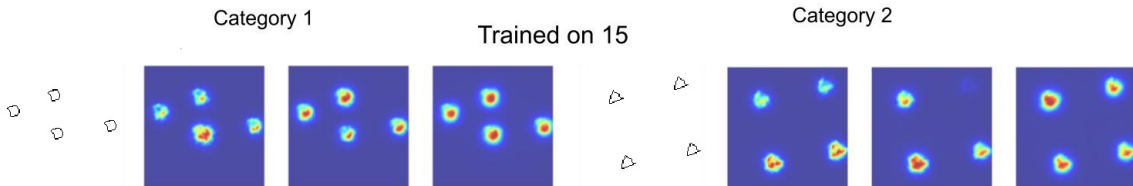


Figure S15: Attribution maps corresponding to the mechanisms learned when training the model on task *15* and testing on task *10*. Rules required in task *15* is to say if the four identical shapes are forming a square or not. Model, when trained on this task *15*, learns to form a square using four shapes in category *2*, so it also solves the task *10*.

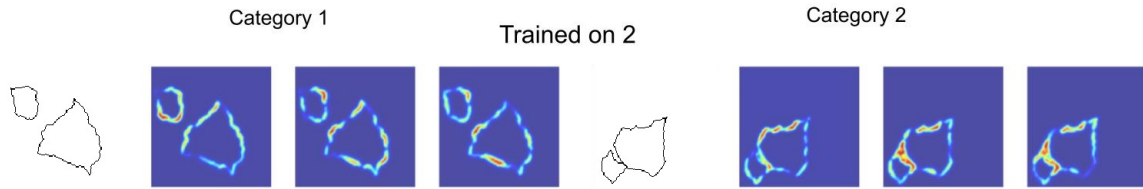


Figure S16: Visual routines learned when training the model when on task 2 is if the two shapes touch from inside or not. We test the model on task 11 where the two shapes are touching from the outside. It shows that the model has learned to recognize touch and use the same relation to solve the task.



Figure S17: Task 21 involves rules related to the geometric transformation related to scaling and rotation. One of the components of this rule is present in task 19 related to scaling, which helps it to understand this task.

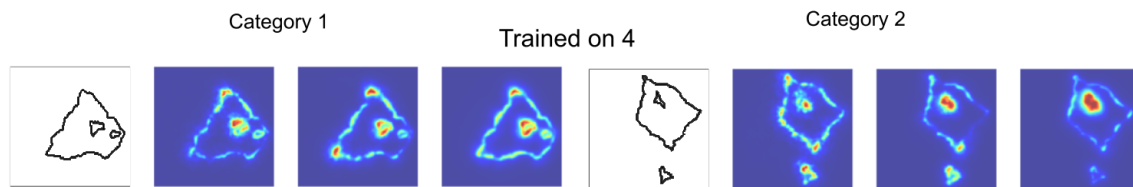


Figure S18: Attribution maps corresponding to the mechanisms learned while training the model on task 4 and testing on images from task 23. In task 4, the model learns the rules to say if one shape is present inside the other or not. This case is true for category 2 of task 23. We expect the model to answer the same even for cases from category 1 where two smaller shapes are present inside the larger shape.

Figure S19: Two representative examples from each category of 23 SVRT tasks Fleuret et al. (2011). Each example has their tasks number labeled in the black box with its description mentioned below.

Figure S20: Two representative examples from each category of 23 SVRT tasks Fleuret et al. (2011). Each example has their tasks number labeled in the black box with its description mentioned below.

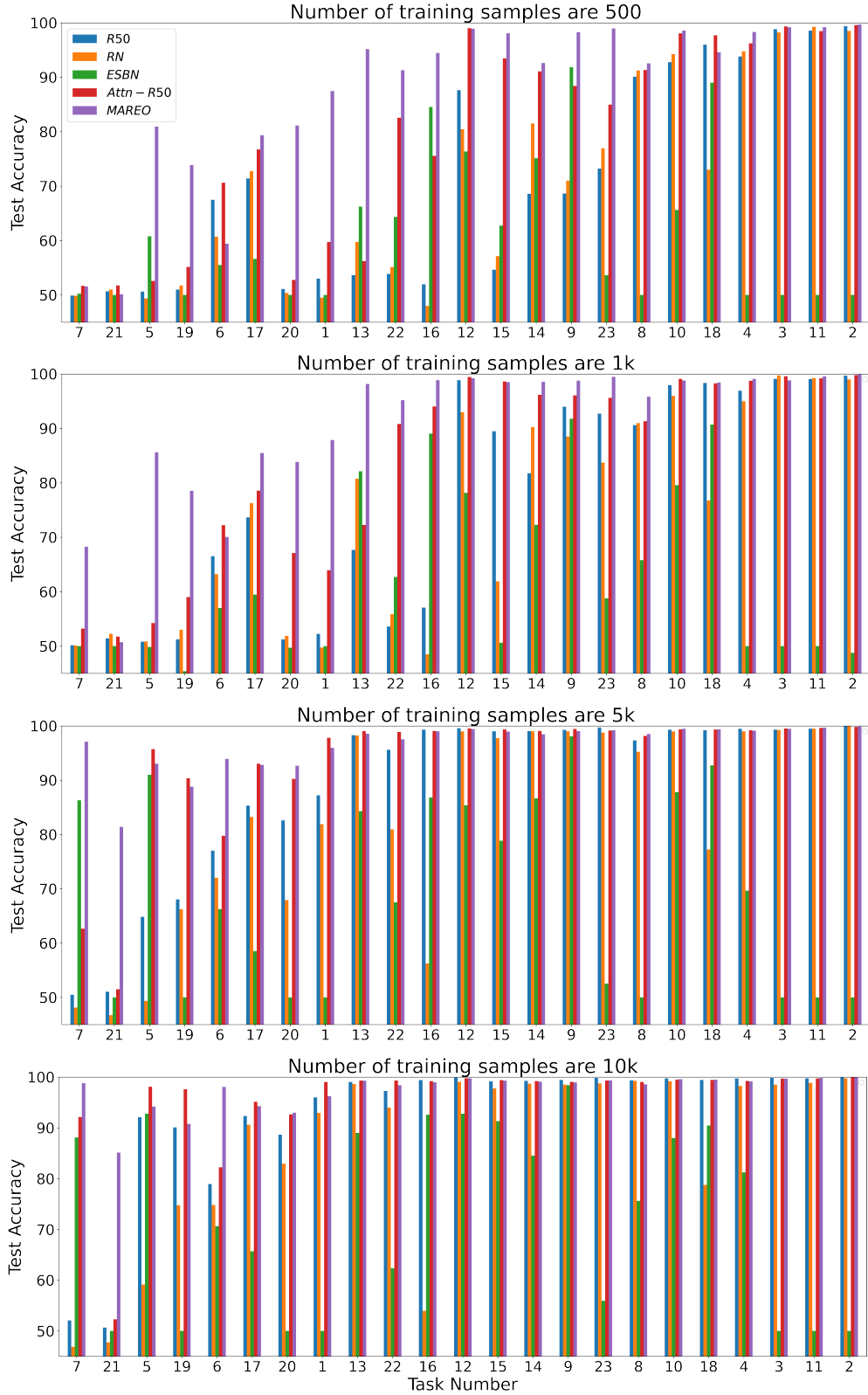


Figure S21: Comparing task level test accuracies of ResNet-50 ( $R50$ ), Relation Network ( $RN$ ), ResNet-50 with attention ( $Attn-R50$ ) and  $MAREO$  for four training set sizes 500, 1k, 5k and 10k. Tasks are arranged as per the taxonomy introduced in Vaishnav et al. (2022) representing the rules involved to define a task. For  $ESBN$  model, task 3, 11 are not evaluated.

## S6 Hyperparameters

**Number of heads** : In order to decide the number of heads of the guided-attention module, we ran experiments on the same-different differentiation task of ART Dataset. For all the four holdout values, we evaluated *MAREO* with a varied number of heads in the multi-head attention module (no. of head = 1, 4, 8, 16) and found that head = 4 (Figure S1) works best for all the holdout scenarios and we fixed this value as 4 for all our experiment.

Table S6: **ART**: Number of training and testing samples used for four different types of tasks.

Tasks		m=0	m=50	m=85	m=95
SD	Training	18,810	4,900	420	40
	Test	990	4,900	10,000	10,000
RMTS	Training	10,000	10,000	10,000	480
Dist3	Training	10,000	10,000	10,000	360
ID	Training	10,000	10,000	10,000	8,640
	Test	10,000	10,000	10,000	10,000

Table S6: **ART**: For four different tasks number of epochs and learning rates (LR) used to train different architectures.

Tasks	m=0		m=50		m=85		m=95	
	MAREO							
	Epoch	LR	Epoch	LR	Epoch	LR	Epoch	LR
SD	50	0.0001	50	0.0005	100	0.0005	200	0.001
RMTS	50	0.00005	50	0.0001	50	0.0005	300	0.0005
Dist3	50	0.00005	50	0.0001	50	0.00005	300	0.0005
ID	50	0.00005	50	0.00005	50	0.0005	100	0.0005
Other baselines								
SD	50	0.0005	50	0.0005	100	0.0005	200	0.0005
RMTS	50	0.0005	50	0.0005	50	0.0005	300	0.0005
Dist3	50	0.0005	50	0.0005	50	0.0005	300	0.0005
ID	50	0.0005	50	0.0005	50	0.0005	100	0.0005

**SVRT** This dataset can be generated with the code <sup>2</sup> provided by the SVRT authors with images of dimension  $128 \times 128$ . No augmentation technique was used for training other than normalization and randomly flipping the image horizontally or vertically, as is customary for this challenge (Vaishnav et al., 2022).

We trained the model for a maximum of 100 epochs with a stopping criterion of 99% accuracy on the validation set. The model was trained using Adam (Kingma and Ba, 2014) optimizer and a binary cross-entropy loss. All the models were trained from scratch. We used a hyperparameter optimization framework *Optuna* (Akiba et al., 2019) to get the best learning rates and weight decays for these tasks and reports the test accuracy for the models which gave the best validation scores.

**Learning compositionality** One of the triplets (21, 19, 25) involves rotation which needed more than 1,000 samples to learn. So, we selected 5,000 samples each from the tasks  $x$  and  $y$  to pre-train the network. This pre-training is carried out for 100 epochs for both tasks. Once the model is trained, we fine-tune it on the novel unseen task  $z$ . We confirmed that *MAREO* was able to learn the new rule with as few as ten samples per category – hence demonstrating an ability to harness compositionality.

## S7 ESNB vs MAREO

We have identified some limitations of the ESNB architecture, such as its sensitivity to translation and noise. It is also incapable in scenarios where there are multiple shapes presented together in the stimulus or if there exist complex relations (Fig. S22).

<sup>2</sup><https://fleuret.org/cgi-bin/gitweb/gitweb.cgi?p=svrt.git;a=summary>

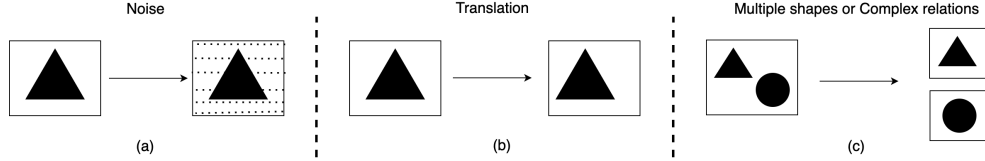


Figure S22: Some scenarios where the memory-based network, *ESBN* (Webb et al., 2021) performs at a chance level which shows the need for explicit attention mechanisms required in addition to memory to build a robust system. (a) Adding any kind of noise to the dataset, (b) If the image is not centered, (c) If there are multiple shapes (or the presence of complex relations like in the SVRT dataset).

To compare our architecture with that of *ESBN*, we analyzed *MAREO* on ART tasks and analyzed *ESBN* on SVRT tasks.

At first, we evaluated *MAREO* on the ART dataset as shown in Fig. S23. In the previous work Webb et al. (2021), each image is passed as an individual image to the *ESBN* model, which is stored in the external memory bank for contemplating the rule, whereas *MAREO* is smart enough to figure out the rules from a single stimulus containing all the characters (Fig. S24). This time we added translation to every character before passing. To take into account all these complexities introduced like numerous shapes, relations, and stimuli altogether, we let our model run for 2 additional time steps ( $t=6$ ) for tasks Dist3 and ID. For these two tasks, for our model to hold up the same level of performance as without translation, it was difficult without increasing the number of time steps. We compared the accuracy of our architecture and found that even in the hardest generalization scenario ( $m=95$ ), it performs relatively well, where 95% of the shapes were held during training. Our model achieves at least 60% test accuracy when trained from scratch using ten different random seeds. The holdout of 95% is relatively hard for *MAREO* as it takes some time for it to develop an attention mechanism.

We have already seen in section 4, that *ESBN* architecture has difficulty contemplating the rules for the SD and RMSTS tasks. To ensure that the updated backbone is not an issue, we ran a similar experiment where we used the same encoder module ( $f_e$ ) as the one proposed in Webb et al. (2021) and obtained a consistent chance level accuracy.

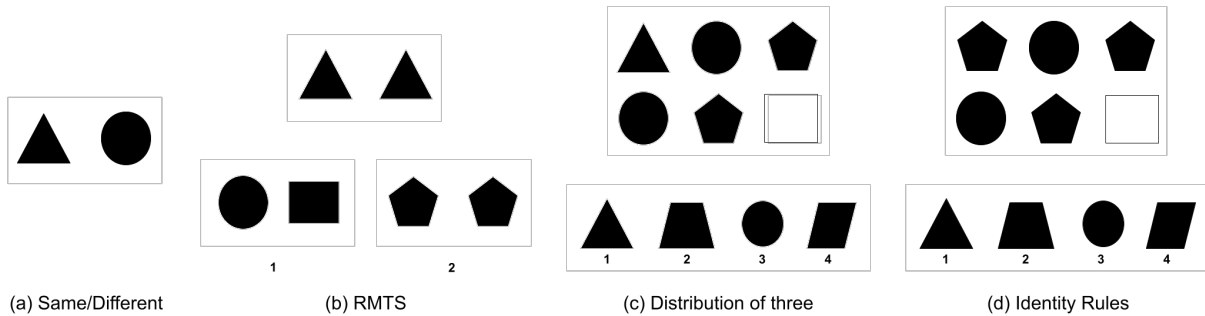


Figure S23: **ART**: (a) Same/different discrimination task. (b) Relational match-to-sample task (answer is 2). (c) Distribution-of-three task (answer is 1). (d) Identity rules task (ABA pattern, answer is 3).

As our next step, we moved on to the part where we analyzed the performance of *ESBN* on SVRT tasks. To make SVRT tasks compatible with the *ESBN* architecture, we disintegrated the shapes of the dataset in different image frames such that their location is intact. We did not center shapes in the dataset as it might alter the rules imbibed in the task because of their spatial relational structure. A representative example of this method can be seen in Fig. S25. Still, two of the tasks (11 and 2) in SVRT cannot be accustomed to this paradigm as they involve the concept of touching. So we skipped those tasks from our analysis because of the complex preprocessing steps involved in separating two touching contours into separate channels.

After this pre-processing step, we pass these individual images to the *ESBN* model and plot the performance in Fig. S21. We found that *ESBN* even struggles with relatively simple tasks that were learned by ResNet50 and other non-attentive models. Such tasks can be solved with approximately 500 samples, whereas *ESBN* did not learn to solve these tasks (14, 9, 23, 10, 2) even after training with 10k samples. We believe that the inability to formulate the spatial relations between

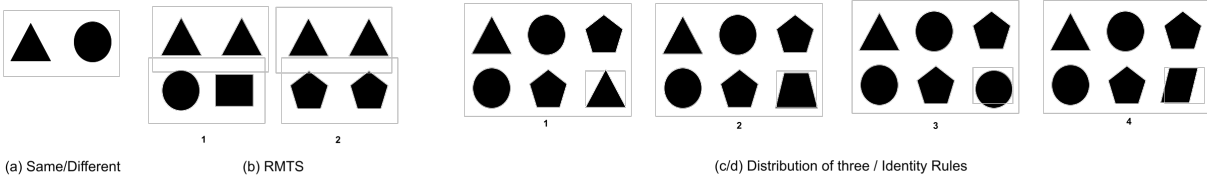


Figure S24: **ART for MAREO**: (a) Same/different discrimination task. (b) Relational match-to-sample task (answer is 2). (c) Distribution-of-three task (answer is 1). (d) Identity rules task (ABA pattern, answer is 3).

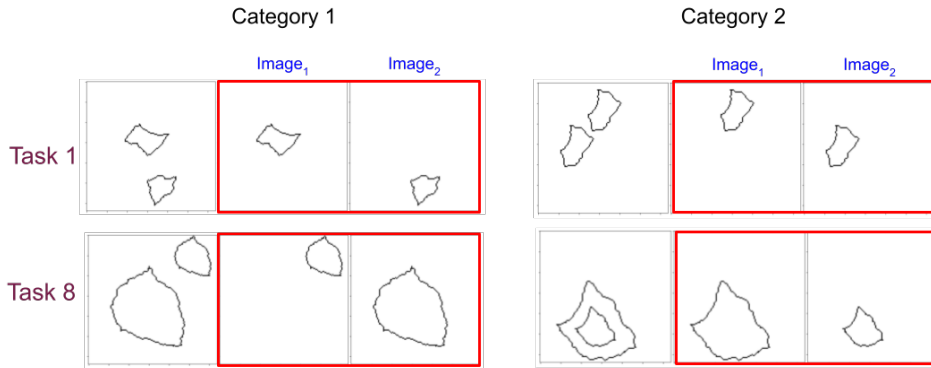


Figure S25: SVRT tasks compatible with ESNB model where each object is separated into individual images and passed to the ESNB in a sequential manner.

shapes presented as individualized images is one of the significant drawbacks of architectures based on object-centric attention like ESNB.

### S7.1 Noise Robustness

In this experiment, we tested the robustness of these two architectures against noise for two different datasets. We selected the most basic task of same-different discrimination (Fig. S23) and used both the architecture in their naturalistic training paradigm. During training and testing, we added Gaussian noise to the images. We found that ESNB is not able to pass chance level accuracy even for the 0-holdout case where all the symbols are presented during the training time, whereas *MAREO* experienced an insignificant drop in accuracy (Fig. S26). We observed a similar trend in the performance when we repeated the same experiment with a complex variant of same-different tasks, i.e., SVRT, and plotted the results in Fig. S27. We matched the number of parameters in the encoder block ( $f_e$ ) in both these experiments.

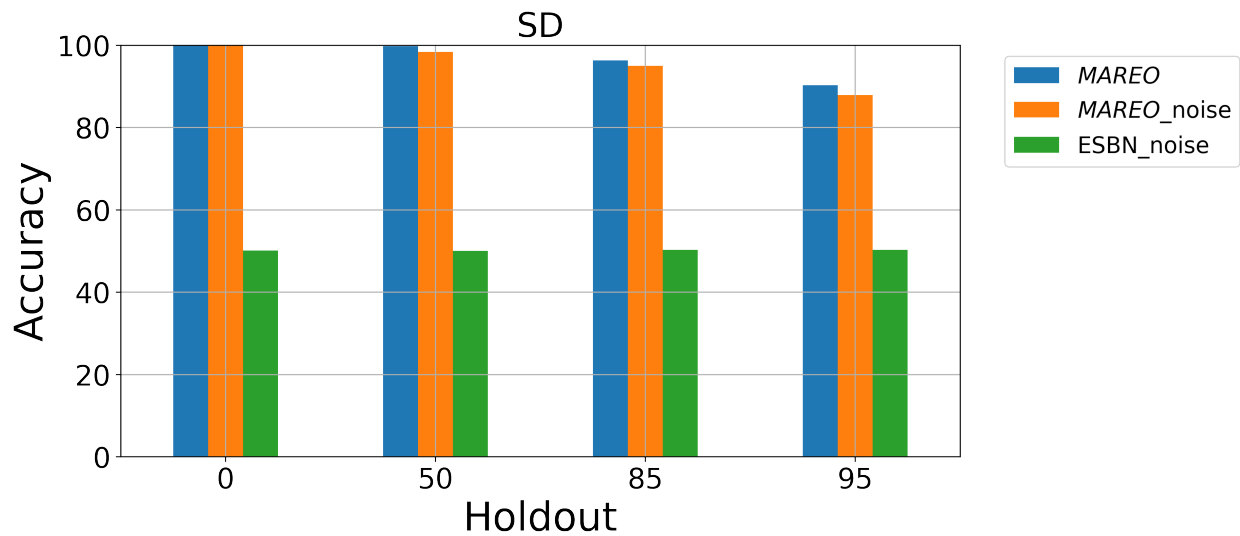


Figure S26: Test accuracy plot for same-different (SD) differentiation task when training and testing *MARIO* with the presence of Gaussian noise with different holdout values. For comparison, we also plot the model’s accuracy without any noise and show an insignificant difference in accuracy between these two cases. However, ESNB struggles to learn at the 0 holdout scenario, thereby representing its inability to attend to shapes because it lacks an attention mechanism.

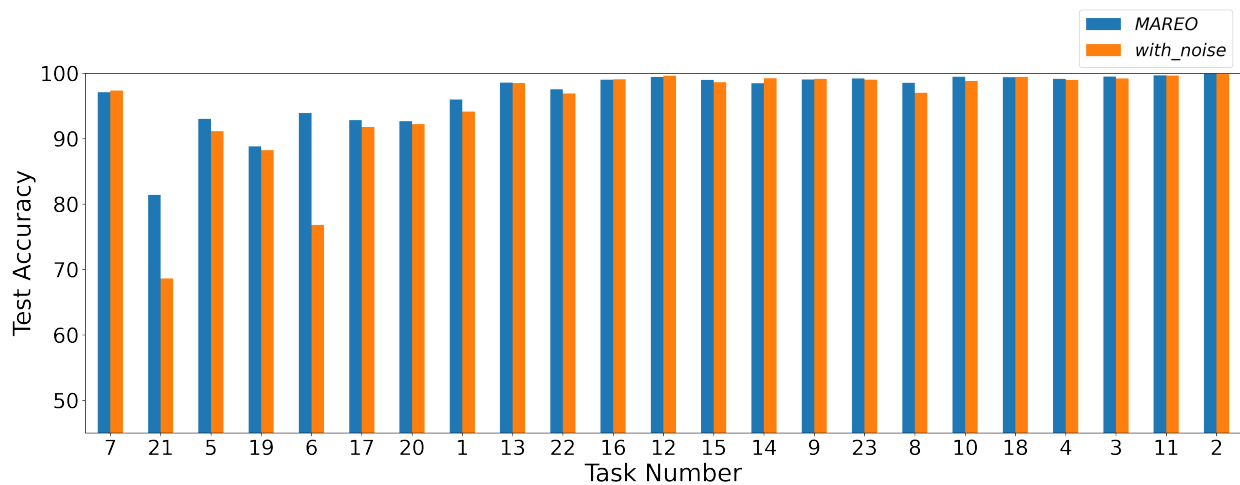


Figure S27: Test accuracy plot when training and testing *MARIO* with the presence of Gaussian noise using 5k samples on all twenty-three SVRT tasks. For comparison, we also plot the model’s accuracy without any noise and show an insignificant difference in accuracy between these two cases.